Constraining plant hydraulics with microwave radiometry in a land surface model: Impacts of temporal resolution

Nataniel Holtzman[1], Yujie Wang[2], Jeffrey. D. Wood[3], Christian Frankenberg[2,4], and Alexandra G. Konings[1]

[1]Stanford University, Department of Earth System Science.

[2]California Institute of Technology, Department of Environmental Science and Engineering.

[3]University of Missouri, School of Natural Resources.

[4]Jet Propulsion Laboratory, California Institute of Technology.

Corresponding author: Nataniel Holtzman (nholtzma@stanford.edu)

Key Points:

- We demonstrate that ecohydrological parameters and variables can be inferred from microwave radiometry via model-data fusion
- We compare scenarios that use synthetic observations at different times of day, corresponding to current and proposed satellite orbits
- For inferring land surface variables, using observations from just four times of day proves to be as useful as using data from every hour

Abstract

Vegetation water content (VWC) plays a key role in transpiration, plant mortality, and wildfire risk. Although land surface models now often contain plant hydraulics schemes, there are few direct VWC measurements to constrain these models at global scale. One proposed solution to this data gap is passive microwave remote sensing, which is sensitive to temporal changes in VWC. Here, we test that approach by using synthetic microwave observations to constrain VWC and surface soil moisture within the CliMA Land model. We further investigate the possible utility of sub-daily observations of VWC, which could be obtained through a satellite in geostationary orbit or combinations of multiple satellites. These high-temporal-resolution observations could allow for improved determination of ecosystem parameters, carbon and water fluxes, and subsurface hydraulics, relative to the currently available twice-daily sun-synchronous observational patterns. We find that incorporating observations at four different times in the diurnal cycle (such as could be available from two sun-synchronous satellites) provides a significantly better constraint on water and carbon fluxes than twice-daily observations do. For example, the root mean square errors (RMSE) of projected evapotranspiration and gross primary productivity during drought periods was reduced by approximately 40%, when using four-times-daily relative to twice-daily observations. Adding hourly observations of the entire diurnal cycle did not further improve the inferred parameters and fluxes. Our comparison of observational strategies may be informative in the design of future satellite missions to study plant hydraulics, as well as when using existing remotely sensed data to study vegetation water stress response.

1 Introduction

The amount of water contained in plant tissues is a key modulator of terrestrial ecosystem function. Plant water status can be quantified as vegetation water content (VWC) or as leaf water potential (ψ_l), which are monotonically related to each other in a given plant (Turner, 1988). During a drought, changes in VWC help determine whether plant mortality occurs and by what mechanism (i.e. carbon starvation or hydraulic failure) it tends to occur (Ding et al., 2021; Martinez-Vilalta et al., 2019; McDowell et al., 2008; Rao et al., 2019). VWC and ψ_l can also help predict how transpiration and photosynthesis respond to drought (Eller et al., 2020; Matheny et al., 2017). Each of these processes depends on plant water use strategy, which can be characterized by analyzing VWC and ψ_l dynamics (Konings & Gentine, 2017; Y. Liu, Konings, et al., 2021; Wu et al., 2021). VWC also reflects plant growth responses to rainfall pulses in semi-arid ecosystems (Feldman et al., 2021; Feldman, Short Gianotti, et al., 2018) and modulation of land-atmosphere interactions (Feldman et al., 2020). Lastly, VWC dynamics strongly affect wildfire activity and burned area (Nolan et al., 2016; Rao et al., 2022; Yebra et al., 2013).

Global monitoring of VWC would improve our understanding of ecosystem resiliency and vulnerability to climate stress, especially considering that ecosystem responses to historical drought vary by region (Z. Yu et al., 2017), in part due to regional differences in the plant traits that modulate VWC dynamics. However, measurements of VWC and ψ_l are typically made in-situ on individual plants (Konings et al., 2019; Novick et al., 2022). It is difficult to scale these measurements up to coarser spatial scales with confidence, because of the high heterogeneity of plant hydraulic strategies within and across ecosystems (Anderegg, 2015; Skelton et al., 2015). Remote sensing can help address this shortcoming, as data from spaceborne sensors are spatially widespread by design (Konings et al., 2021; Steele-Dunne et al., 2012). Out of the many

wavelengths used for remote sensing, microwave observations are particularly sensitive to water content, both in the soil surface and in vegetation (Ulaby & Long, 2014).

The effect of vegetation moisture on microwave observables is typically characterized as vegetation optical depth (VOD), which is approximately linearly related to the total canopy water content in the area (Jackson & Schmugge, 1991). Total canopy water can be expressed as the product of aboveground biomass times VWC. In turn, through an ecosystem-scale (and ecosystem-specific) pressure-volume curve, VOD can be interpreted as an indirect indicator of ψ_l (Konings et al., 2019). Recent field and data-driven studies have shown that VOD is indeed sensitive to changes in leaf water potential on hourly, daily, and seasonal time scales (Holtzman et al., 2021; Momen et al., 2017).

Based on the sensitivity of VOD to leaf water potential, VOD can be used as a constraint on plant hydraulics in a land surface model. In addition to aiding our ability to monitor and predict plant hydraulic responses to climate, such model-data fusion has been proposed as a way to estimate belowground water uptake, which is very difficult to measure directly (Konings et al., 2021; Y. Liu, Konings, et al., 2021). This approach is distinct from (and could be complementary to) assimilating VOD into an ecosystem model as a constraint on biomass (Kumar et al., 2020).

Liu et al (2021) fused satellite data with a simple land surface model to estimate globally resolved maps of plant hydraulic traits. That study found large between-trait differences in the ability of VOD data to constrain those traits. Using synthetic data to test the ability of their approach to retrieve traits, they found that the correlations between prescribed and retrieved values ranged from 0.46 to 0.96 among the seven traits they retrieved. Retrievals using observed VOD also showed significant uncertainty. Many factors could contribute to these uncertainties, including the model accuracy, the inherent sensitivity of the model outputs to each trait, the prior distribution used for each trait in the model-data fusion algorithm, the observation operator that connects ψ_l with VOD (Shan et al., 2022), and the temporal availability of the remote sensing observations. It is unclear which factors are primarily responsible for the residual uncertainty and for the lack of constraint on certain traits.

In this study, we investigate one avenue for potentially improving microwave remote sensing constraints on ecosystem dynamics: the temporal frequency of observations. Existing satellites carrying passive microwave sensors are typically in sun-synchronous orbits. This orbit type produces a repeat cycle where the satellite passes over a given point on Earth at two fixed times of day, 12 hours apart. For example, the Soil Moisture Active Passive satellite (SMAP) has overpass times of 6 AM and 6 PM, revisiting every 1 to 3 days depending on latitude (Entekhabi et al., 2010). As a second example, the Advanced Microwave Scanning Radiometer 2 (AMSR2), has overpass times of 1:30 AM and 1:30 PM, with revisits every 1 to 2 days (Kachi et al., 2014; Kim et al., 2018).

Viewing a location at two fixed times of day provides only limited snapshots of the full dynamics of plant hydraulic status. Furthermore, for a sun-synchronous orbit those snapshots are 12 hours apart, so they will rarely capture the full diurnal amplitude of leaf water potential, which tends to have a daily maximum just before dawn and daily minimum in early afternoon, approximately eight hours apart (Katerji et al., 1986; Klepper, 1968). Nelson et al. (2018) found that the shape of the diurnal cycle of transpiration is an indicator of drought stress, which suggests that sub-daily VWC observations may enable improved characterization of drought stress. Such observations may also improve transpiration predictions, as many land surface

models fail to capture the VWC-related hysteresis that has been observed in the diurnal cycle of transpiration relative to the cycles of vapor pressure deficit and solar radiation (Matheny et al., 2014; Renner et al., 2019). The degree of hysteresis is modulated partly by atmospheric variables (vapor pressure deficit and radiation), but also by vegetation hydraulic strategy and root-zone soil moisture, which could both potentially be constrained by passive microwave remote sensing (S. Xu et al., 2022; Zhang et al., 2014).

Unlike a sun-synchronous orbit, a geostationary orbit provides near-continuous observations in time (revisit time under 1 hour) over a fixed field of view. Geostationary satellites are widely employed for weather monitoring, but their data have also been recently used to constrain land surface processes (Khan et al., 2021). For example, Xu et al. (2018) estimated daily sensible and latent heat fluxes based on full diurnal cycles of land surface temperature from the Geostationary Operational Environmental Satellite (GOES) constellation. Xiao et al. (2021) provide an overview of upcoming geostationary satellite missions and their potential for studying ecosystem stress responses.

Konings et al. (2021) recently proposed two options for next-generation remote sensing of VWC: a geostationary satellite or a constellation of several small satellites (smallsats) with different orbits and thus different overpass times. The relevance of smallsat constellations to data assimilation is also discussed in Kumar et al. (2022). If eventually launched, the increased temporal resolution of these new mission concepts might improve our ability to constrain plant hydraulic traits and ecosystem dynamics. On the other hand, geostationary satellites are particularly expensive to engineer and launch since they orbit at a much greater distance from the Earth than satellites in sun-synchronous orbits. Thus, it is essential to determine how much benefit the increased information from possible new satellites would provide to scientific applications.

Here, we investigate that question: would observations throughout the day provide improved model performance and trait identification when fused with a land surface model? Or would they simply "connect the dots" in a consistent and predictable way between the existing twice-daily observations, providing no overall increase in information content? To quantify the potential utility of different observational frequencies, we use a simulation experiment. The simulation setting allows the sources of error in observations to be controlled, so that temporal frequency is the only difference between the experimental scenarios. We limit our focus here to passive microwave remote sensing (radiometry) rather than active (radar), because the physical processes relating VWC and remote sensing observables are better understood for radiometry than for radar (Konings et al., 2019; Shan et al., 2022).

In this study, we compare the utility of data that is available twice daily (analogous to a sun-synchronous orbit), four times daily (combining data from two satellites), or hourly (a geostationary orbit). We use Bayesian model-data fusion to infer plant hydraulic trait values from simulated remote sensing observations at these temporal frequencies. Because models with many parameters typically exhibit equifinality (Khatami et al., 2019; Tang & Zhuang, 2008) and because the observables are typically more sensitive to some parameters than other parameters, the accuracy of the retrieved trait values themselves does not tell the full story of whether the retrieved parameters accurately describe the ecohydrological system being studied. Thus, we also use the retrieved trait values to predict ecosystem responses to drought, focusing on soil moisture, evapotranspiration and gross primary productivity as variables of interest. We analyze

differences in the accuracy of these predicted ecosystem dynamics (relative to the original reference model run) across the different observational scenarios.

2 Materials and Methods

2.1 Experimental Design

Our study takes the form of an Observing System Simulation Experiment (OSSE), a simulation study in which retrieval algorithms are tested on simulated (but realistic) satellite observations to assess the accuracy of the environmental inference, which is associated with a known truth. The goal of an OSSE is to assess quantitatively how much information could be gained about an environmental process from a specific type of observation system (Arnold & Dey, 1986; Zeng et al., 2020). Here, we run different versions of the same OSSE to assess how changing microwave observational frequency affects the accuracy of the inferred ecohydrological fluxes and water pools. Since an OSSE is based on simulations of both the underlying environmental processes and the observing system (as opposed to using real observations), it does not require that the observing system be operational yet, and thus can be used to plan future observing systems (Atlas, 1997).

The steps in our experiment are summarized in Fig.1. We started by running a land surface model (described in Sect. 2.2) to create simulated time series of ecosystem states and fluxes over 13 years (2005 through 2017). This model run used prescribed parameter values for plant and soil hydraulic traits. For the rest of the study, we treated the parameter values and model states from the original model run as a synthetic "truth" scenario. We then used a simple radiative transfer model (described in Sect. 2.3) and added noise to simulate realistic observations of horizontally and vertically polarized microwave brightness temperature for one year (2007), based on the land surface model outputs of surface soil moisture and vegetation water potential. We only used one year of simulated observations, rather than multiple years, due to the computational cost of the model-data-fusion algorithm. We picked the year 2007 for this purpose because it includes substantial water stress, but not the highest water stress of the entire dataset, which occurs in 2012.

We ran several parallel experiments, each with a different temporal arrangement of observations corresponding to a different satellite orbit scenario, determining the retrieved traits and associated fluxes for each scenario:

- "HOURLY" – observations 24 hours a day, every day (This represents a geostationary satellite.)
- "1 AM/PM" – observations at 1 AM and 1 PM, every third day (This represents the type of data currently available from AMSR-E)
- "6 AM/PM" – observations at 6 AM and 6 PM, every third day (This represents the type of data currently available from SMAP)
- "1+6" – combination of 6 AM/PM and 1 AM/PM, with the four combined observations all coming on the same day of each 3-day cycle (This represents a combination of two satellites with different overpass times)

Figure 2 shows an example time series of VOD from the "true" model, and how each observation scenario views the same time series differently due to temporal frequency.

Based on each temporal subset of simulated observations over the 1-year observing period, we used a Markov chain Monte Carlo (MCMC) model-data fusion algorithm (described in Sect. 2.4) to retrieve Bayesian estimates of the land surface model parameters. For each scenario, we then took 120 samples from the estimated joint posterior distribution of parameters, and ran the land surface model for the full 13 years using each sampled parameter set. This procedure generates an ensemble of retrieved model runs that can be compared to the "true" model run. To illustrate the results of this methodology, Fig. S1 shows the water potential over a few days for a subset of the retrieved ensemble.

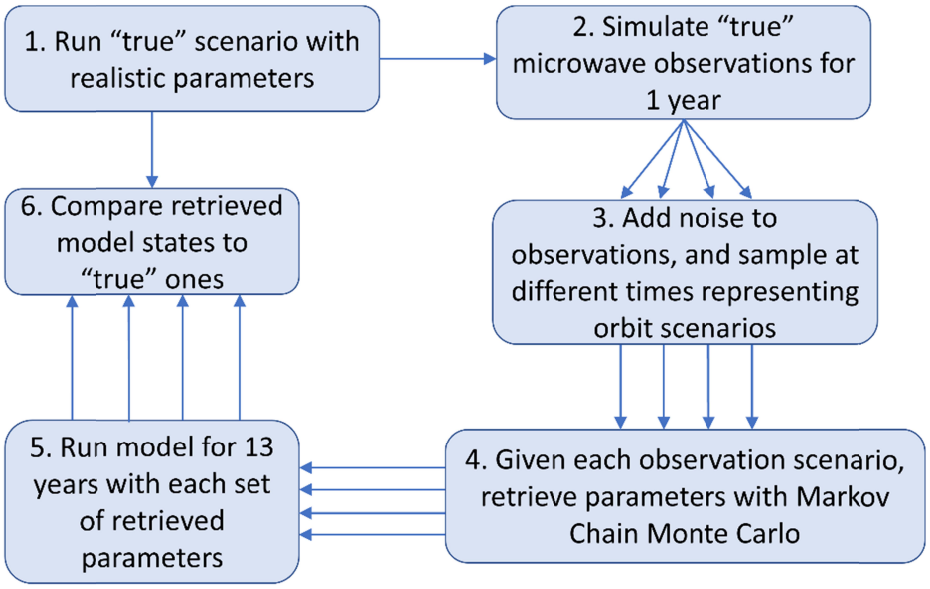

Figure 1. Schematic illustrating the overall framework of our simulation experiments. The sets of four parallel arrows represent the four observation scenarios.

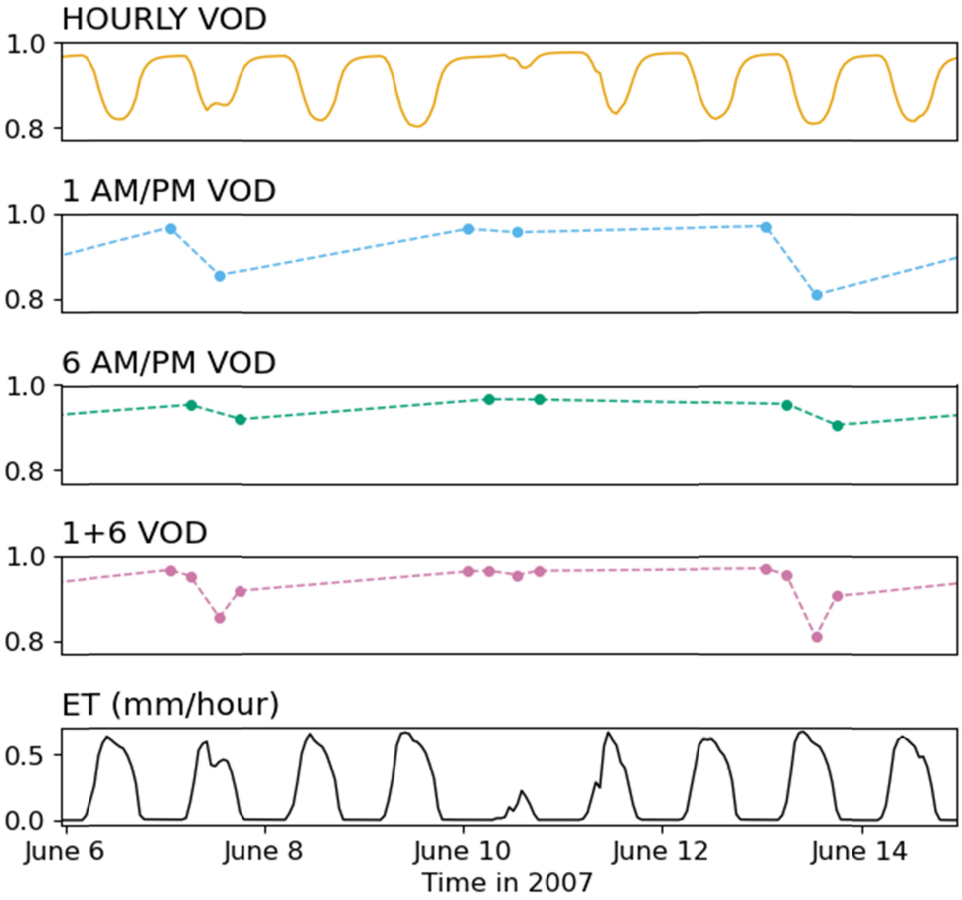

Figure 2. Example time series of how the four observation scenarios sample VOD in time. Model output ET is also shown for reference. Note that in our model-data fusion process, it is brightness temperatures, rather than VOD, which are directly combined with the model

Aside from the single year that was "observed" to retrieve the parameters, the 13-year evaluation period represents unseen inputs from the point of view of the retrieval algorithm. Evaluating the model behavior over this period is distinct from simply evaluating the accuracy of the retrieved parameters. Like real ecosystems, our model includes nonlinear processes that become especially important during drought; the xylem vulnerability curve is one example. In a year without climate stress, the effect of those processes on remote sensing observations of the ecosystem might be so small as to be masked by noise, so that observations during that year would not be useful for constraining the parameters governing those processes. We are interested in whether more frequent observations can help "unmask" those parameters. We intentionally did not include the most extreme drought year (2012) in the "observation" period, so that the model would have to predict ecosystem behavior under more extreme stress than it encountered when retrieving the parameters. This arrangement is relevant to practical applications, since ecosystem responses to extreme events are often of interest, but may not be present in the relatively short observational record and may become more likely with climate change (Frank et al., 2015; Reyer et al., 2013).

Over the evaluation period, we assessed the accuracy of several key model variables – leaf water potential (ψ_l), soil moisture, evapotranspiration (ET), and gross primary productivity

(GPP) – by calculating the root mean square error (RMSE) of each retrieved ensemble member relative to the "true" model run. In this analysis, we used the vertically integrated soil moisture over the entire soil column, not just the surface soil moisture that directly affects the microwave brightness temperature. For each observation scenario and each model variable, we obtained a probability distribution of RMSE over the posterior retrieved parameter distribution. We compared the RMSE distributions of the different observation scenarios using a Mann-Whitney U test (a non-parametric analog to a t-test). We also calculated other error metrics (correlation and bias) to analyze the reasons for model performance differences between the observation scenarios.

In addition to predicting ecosystem behavior during typical conditions, it is also important to characterize responses to climate extremes. Thus, we repeated the RMSE analysis, but instead of using 13 full years in the error calculation, we limited the analysis to the four summers with the lowest total precipitation (aside from the 2007 model-data fusion year): 2005, 2012, 2013, and 2014. Here, summer was defined as June 1 through September 30.

2.2 Model Structure

Previous work on using VOD to constrain plant hydraulics with model-data fusion has used simple models built specifically for that purpose (Y. Liu, Holtzman, et al., 2021). In the past few years, full-fledged land surface models – of the type that are used in global climate and weather modeling – have begun to include water potential as a prognostic variable (Eller et al., 2020; Kennedy et al., 2019; L. Li et al., 2021), raising the possibility of using VOD to constrain the hydraulics of land surface model. Here, we investigated model-data fusion in a new land surface model (CliMA Land) that includes a sophisticated treatment of plant hydraulics (Y. Wang et al., 2023).

The land surface model used in this study is derived from the CliMA (Climate Modeling Alliance) Land model, including the SoilPlantAirContinuum, Photosynthesis, and StomatalModels modules (Y. Wang et al., 2021). The model represents vegetation in analogy with a tree, with several organs: roots, trunk, branches, and leaves (Fig. 3). The single trunk is connected at its base to several roots that extend down into different soil layers, and it is connected at its top to several branches that extend up to different heights. Each branch is connected to a leaf, and each leaf contains a sunlit part and a shaded part (not shown in Fig. 3 for simplicity). Each canopy layer, comprising a branch and shaded/sunlit leaves, is connected to a layer of air. The model can contain an arbitrary number of canopy layers to model gradients of light within the canopy; however, in this study we only use three canopy layers for reasons of computational efficiency.

The processes and variables that are simulated prognostically in our model include: optical radiative transfer through the canopy, transpiration and photosynthesis in leaves, water potential and water content in each plant organ, water flow between connected plant organs, water uptake from soil to roots, vertical drainage through the soil, and runoff. Variables that are prescribed from external data include leaf area index (LAI), and meteorological data (precipitation, air temperature, humidity, and incoming solar radiation at the top of the canopy).

In each time step of the model, the following processes occur:

- The transfer of light within the canopy is modeled based on incoming photosynthetically active radiation, leaf area index, and the vertical locations of leaf layers.
- For each leaf layer, photosynthesis and stomatal conductance are modeled, yielding values of transpiration and carbon assimilation.
- A non-steady-state plant hydraulics scheme models water flow, water storage, and water potential within the plant.
- The soil moisture in each soil layer is updated to account for vertical drainage, precipitation, root water uptake, and runoff.

We added steps 3 and 4 specifically for the purposes of our study, beyond the SoilPlantAirContinuum module, while steps 1 and 2 are implemented similarly to the work of Y. Wang et al. (2021). We use the two-leaf radiative transfer model based on sunlit and shaded big leaves. Photosynthetic carbon assimilation is modeled using the Farquhar model (Farquhar et al., 1980). Furthermore, in the photosynthetic step we attempted to mimic a realistic situation where the observational data contains processes that are not represented completely correctly in the model, by forcing the retrieval algorithm to work with a parametrization that is not completely representative of the "true" model. Specifically, we used two different stomatal conductance schemes: the "true" model uses the Medlyn scheme while the retrieval algorithm used the Ball-Berry scheme (Ball et al., 1987; Medlyn et al., 2011). This difference prevents the retrieval algorithm from being able to perfectly replicate the "true" model,

In Step 3 of the model, we implemented a new non-steady-state plant hydraulics scheme within CliMA Land. We introduce a capacitance-related parameter V (specifically, the total water volume stored by the plant at saturation). This parameter allows the model to represent a spectrum of possible plant hydraulic strategies beyond a simple steady-state assumption. Our scheme uses a governing equation based on Darcy's law, as in the FETCH2 plant hydraulic model (Mirfenderesgi et al., 2016; Silva et al., 2022). Unlike FETCH2, here we did not attempt to model gradients of water potential over the length of the vegetation components. Instead of a partial differential equation (PDE), our model is formulated as a system of ordinary differential equations (ODEs), with one differential equation for each leaf, each branch, the trunk, and each root. Details of the plant hydraulic model and its linkage with stomatal function are described in the Supplemental Information Sect. S1 and S2.

In Step 4 of the model, we use the Van Genuchten equation to parametrize the soil water retention curve and the Richards equation to model water drainage through the soil (M van Genuchten, 1980; Tindall et al., 1999). There are eight soil layers in our model, with layer thicknesses increasing from top to bottom. A constant head boundary condition is assumed at the bottom of the soil column, as in the soil-plant-atmosphere continuum model of Liu et al (2017). Water runs off through saturation excess in the top layer and through drainage at the lower boundary.

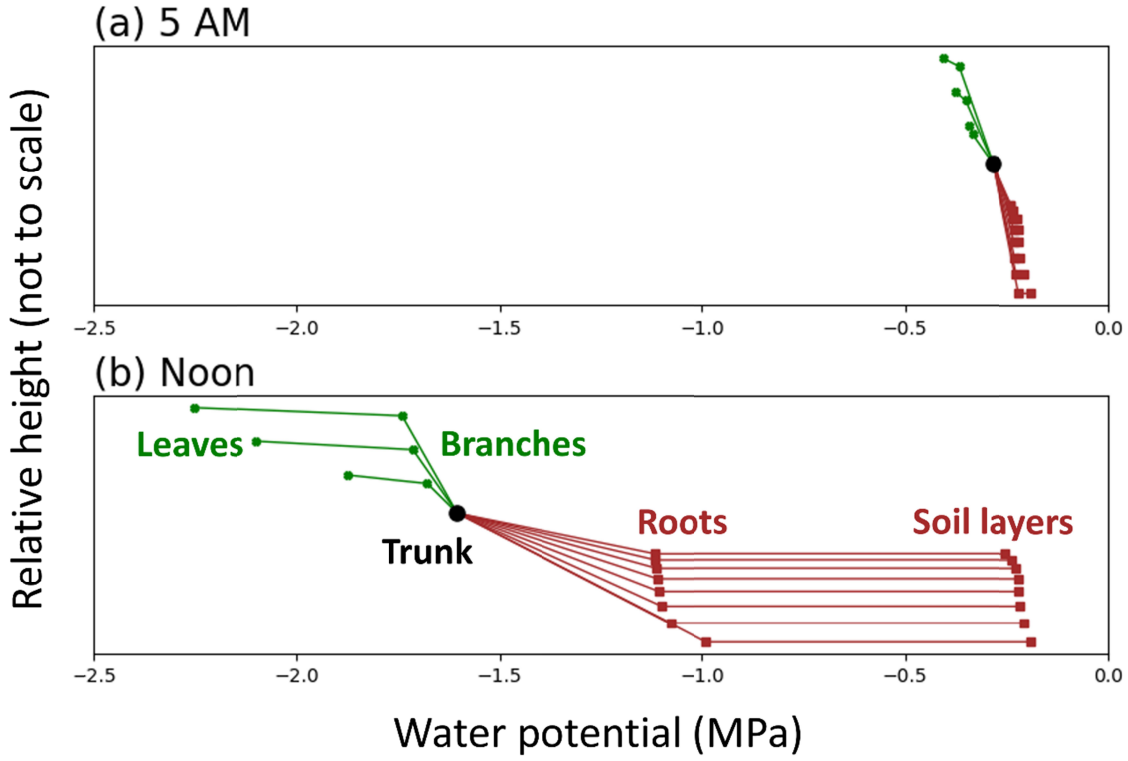

Figure 3. Schematic of plant organs as represented in CliMA Land using sample, illustrative water potential values at two times of day.

2.3 Model Parameters

The model parameters that we retrieve from synthetic remote sensing observations are summarized in Table 1. Sect. S3 summarizes other model parameters that were not retrieved in this study but rather treated as known. Of the retrieved parameters, seven were related to plant traits and six were related to the soil. Our inclusion of a variety of soil parameters was motivated by the finding of Novick et al. (2022) that land surface model behavior is quite sensitive to soil parameter values. Furthermore, soil water retention curve parameters are not typically known a priori, but predicted from soil texture using pedotransfer functions that have large uncertainties (Novick et al., 2022; Vereecken et al., 2022).

The prescribed "true" values of the retrieved parameters were chosen to represent a temperate deciduous forest, using the rich ecological and physiological data available from the oak and hickory dominated Missouri Ozarks Ameriflux (MOFLUX) site to prescribe parameter values when possible (Gu et al., 2016; J. D. Wood et al., 2023). Soil depth was chosen to be within the range of what is observed at the MOFLUX site (J. Wood & Gu, 2022). Soil hydraulic conductivity was chosen based on a typical value for the soil type found at the site, Weller silt loam soil (Young et al., 2001). The soil water retention curve was fitted to laboratory measurements on soil collected at the MOFLUX site (J. Wood et al., 2022). A value for maximum xylem water storage volume was chosen using biomass data from another site (Harvard Forest), with this value assumed as a typical biomass for temperate deciduous forests, and assuming equal proportions of dry wood and water at saturation (Munger & Wofsy, 2020).

Other parameter values were manually tuned so that the land model approximately matched the observed magnitude, seasonality, and interannual variation of ET, GPP, column-averaged soil moisture, and pre-dawn ψ_l at the MOFLUX site (Pallardy et al., 2018; J. Wood & Gu, 2022). Leaf area index (LAI) was prescribed as an input time series, though future versions of the CliMA model may include prognostic LAI within the model itself. We selected LAI data at the pixel over the MOFLUX site from the Moderate Resolution Imaging Spectrometer (MODIS) satellite (Myneni et al., 2002). We then adjusted the MODIS data's mean, amplitude, and seasonal timing to match in-situ LAI observations from the MOFLUX site. Because there were several time gaps in the in-situ LAI observations, we did not use them as direct inputs to CliMA.

Figure 4 demonstrates the model's realistic behavior by comparing model outputs with observed time series from eddy covariance and predawn ψ_l measurements. It should be noted that, as this study is an OSSE, our goal was not to perfectly calibrate a land surface model to a specific site, but rather to investigate model-data fusion with synthetic remote sensing data. We simply used the MOFLUX observations as a starting point to ensure the behavior of the new CliMA Land version was ecologically plausible.

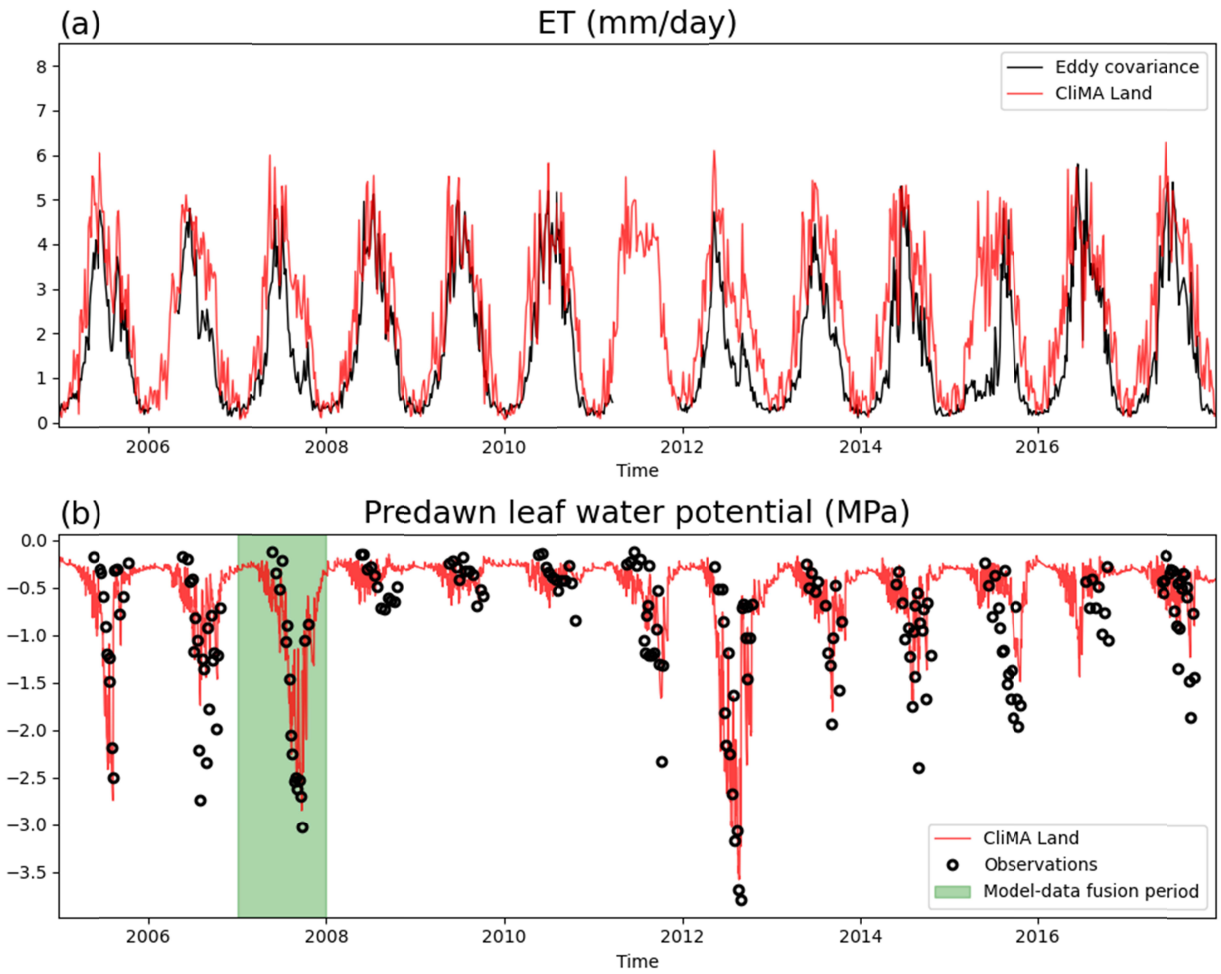

Figure 4. Comparison between "true" CliMA Land simulation and observations at the MOFLUX site for: (a) 5-day average ET, and (b) predawn leaf water potential. For reference, the one-year model-data fusion period during which we used synthetic remote sensing observations is shown in green.

Table 1. Parameters retrieved from simulated observations. A flat non-negative prior is used for the radiative transfer parameters. The other prior distributions are log-uniform. Note that the Medlyn model g_1 parameter is only used in the "true model," not in the retrieval, so it does not have a prior distribution. Also, $P63_x$ is parametrized in the MCMC as an additive constant plus the value of $P63_\beta$.

Parameter name and symbol	Units	Normalized by ψ_{ref}?	True value	Prior range
Radiative transfer parameters				
Single scattering albedo (ω)	-	no	0.05	(0, ∞)
Sensitivity of VOD to leaf water potential (a)	MPa^{-1}	yes	0.067	(0, ∞)
Contribution of woody biomass to VOD (b)	-	no	0.81	(0, ∞)
Sensitivity of VOD to LAI (c)	-	no	0.051	(0, ∞)
Stomatal parameters				
Maximum carboxylation rate (V_{cmax})	µmol/s per m^2 of leaf area	no	90	(10, 300)
g_1 in Medlyn model	$Pa^{1/2}$	no	300	N/A (see caption)
g_1 in Ball-Berry model	-	no	N/A	(1, 120)
$P63_\beta$	MPa	yes	-3	(-0.75, -15)
Xylem parameters				
Whole-plant maximum xylem conductance (k_{plant})	mol/s/MPa per m^2 of basal area	yes	10	(0.1, 50)
Whole-plant maximum water storage volume (V)	kg per m^2 of ground area	yes	12	(0.12, 120)
$P63_x$	MPa	yes	-4	(0.01,10) + $P63_\beta$
Soil parameters				
Soil depth (Z)	mm	no	2000	(500, 3000)
Soil moisture lower boundary condition (s_{lower})	m^3/m^3	no	0.4	(0.3, 0.5)
Rate of exponential decrease for rooting profile (α_{root})	m^{-1}	no	2	(0.01, 5)
Shape parameter of soil water retention curve (n)	-	no	1.5	(1.1, 1.9)
Water potential of soil with moisture of 0.21 (ψ_{ref})	MPa	N/A	-1	(-0.125, -8)
Saturated soil hydraulic conductivity (k_{soil})	µm/s	yes	0.4	(0.05, 20)

2.4 Forward model for synthetic remote sensing observations

Our synthetic simulation study used microwave brightness temperatures directly in the model-data fusion process, rather than using VOD and soil moisture data that has been retrieved from brightness temperature through an offline algorithm, to avoid errors due to any inaccuracies of such an algorithm. This approach is consistent with the notion of directly assimilating satellite observables instead of derived products, as advocated in two recent review papers (Kumar et al., 2022; MacBean et al., 2022). When using microwave data as a constraint on soil moisture, De Lannoy and Reichle (2016) found that it was advantageous to directly assimilate brightness temperatures into a land surface model, instead of assimilating soil moisture estimates derived from those brightness temperature. Here, we extended that concept to view brightness temperature as a joint constraint on soil moisture and plant hydraulics.

To simulate the propagation of microwaves near the land surface, we used the tau-omega zeroth-order radiative transfer model, which simulates brightness temperature as a function of the soil surface dielectric constant and the VOD (Mo et al., 1982; Ulaby & Long, 2014). The predicted brightness temperature depends on the single-scattering albedo, ω. Values of ω estimated from real satellite observations have considerable spatial variability even within land cover types (Konings et al., 2017). We thus treated ω as an unknown to be estimated from the observations. For the initial "truth" model, ω was set to 0.05, the value used by the SMAP algorithm for temperate deciduous forests (O'Neill et al., 2019). Calculating brightness temperature also requires the physical temperatures of the soil and canopy. In this study we assumed these temperatures are known with perfect accuracy from external data. Future versions of the CliMA Land model will include prognostic soil and canopy temperatures, which would enable bypassing that assumption by using physical temperature outputs from the model itself.

We used the Mironov dielectric mixing model (Mironov et al., 2002) to parametrize the soil dielectric constant as a function of the land model's surface soil moisture. The dielectric model also depends on the clay content of the soil, which is 15% at the MOFLUX site (J. Wood & Gu, 2022). The effect of surface roughness on the soil reflectivity is parametrized based on the SMAP algorithm (O'Neill et al., 2019) and treated as known.

Plant water content affects microwave brightness temperature through VOD. We modeled VOD in the same way as several previous studies (Holtzman et al., 2021; Y. Liu, Holtzman, et al., 2021; Momen et al., 2017), as a function of leaf water potential (ψ, output by the land surface model) and leaf area index (LAI, prescribed by the forcing input data):

$$VOD = (1 + a\psi_l)(b + cLAI) \qquad \text{Eqn. 1}$$

Above, a, b, and c are constant parameters, which vary between species and ecosystems. The first term, containing leaf water potential (ψ_l), represents VWC (and is mathematically equivalent to VWC here, since our plant hydraulic model assumes a linear pressure-volume curve). The second term, containing LAI, represents above-ground biomass (b represents the effect of woody biomass that does not change over time). As in Liu et al. (2021), we treated these VOD parameters as unknowns to be estimated from microwave observations. Since CliMA Land represents an ecosystem comprised of multiple canopy layers and plant organs with differing water potentials, we must make an assumption about the layers/organs to which VOD is most sensitive. For example, in Eqn. 1, does ψ_l represent leaf water potential at the top of the canopy, averaged throughout the canopy, or some combination of leaf and stem water potential? Here, we used the average leaf water potential of the canopy layers, to represent short-

418 wavelength microwave observations (e.g. X-band), which are relatively insensitive to the woody
419 parts of vegetation (X. Li et al., 2021). However, further research on the relationship of VOD
420 and ψ of different components is needed to determine the accuracy of this assumption.

421 The "true" VOD parameters (*a, b,* and *c*) were tuned to approximately match the local
422 dynamics of remotely-sensed X-band VOD, using the Land Parameter Retrieval Model (LPRM)
423 product based on data from the AMSR-E and AMSR2 satellites (Y. Y. Liu et al., 2011). At the
424 scale of this dataset's 51-by-29 km pixel size, the area of central Missouri immediately
425 containing the MOFLUX site is a heterogeneous mix of forest and cropland, making its VOD
426 difficult to interpret. Thus, to avoid representativeness error, we used LPRM data from a more
427 homogeneously forested area in southeastern Missouri (Mark Twain National Forest,
428 approximately 200 km away from MOFLUX) when tuning the "true" VOD parameters. A
429 comparison of our model outputs with LPRM data is shown in Fig. S2.

430 ### 2.5 Retrieval algorithm

431 To accomplish the inverse process of model-data fusion – estimating the model
432 parameters that best match the observations – we used a Markov Chain Monte Carlo (MCMC)
433 approach. MCMC produces Bayesian estimates of model parameters, based on the likelihood of
434 producing the observations given the parameters as well as prior probability distributions for the
435 parameters. Compared to optimization methods that only retrieve point estimates of parameters,
436 MCMC algorithms sample from the full joint distribution of parameters informed by data (the
437 posterior distribution), permitting easier characterization of parameter trade-offs, equifinality,
438 and uncertainty. The specific variety of MCMC algorithm we used was an Adaptive Metropolis-
439 Hastings algorithm (Haario et al., 2001). Within the algorithm we normalized the log-likelihood
440 of brightness temperature by the number of data points in each observation scenario, so that the
441 only difference between scenarios is *when* the observations occur, not *how often* they occur.

442 We assumed that the observational noise in brightness temperatures follows a
443 normal distribution with zero mean, a known standard deviation, and no temporal
444 autocorrelation, and that the distribution of noise is identical and independent between the two
445 polarizations. The standard deviation of the noise was set at 1.3 K, the observational uncertainty
446 of the SMAP radiometer (Chan et al., 2016).

447 Within the MCMC algorithm, we reparametrized the model by log-transforming the land
448 surface parameters, and also normalizing certain parameters; preliminary tests showed that
449 without this normalization the MCMC chains converged much more slowly. For example, the
450 parameter $P63_\beta$ is normalized by dividing it by the parameter ψ_{ref}, the water potential of soil with
451 a volumetric moisture of 0.21 (the soil moisture that corresponds to a water potential of -1 MPa
452 for the "true" model's water retention curve). Furthermore, to compare values of leaf water
453 potential in retrievals with greatly varying soil water retention curves, we also normalized ψ_l in a
454 similar way. The normalization procedure is described in more detail in Sect. S4. The MCMC
455 implementation is described in more detail in Sect. S5.

456 ## 3 Results

457 ### 3.1 Comparison of retrievals with synthetic observations

458 Fusing hourly synthetic brightness temperatures with the CliMA Land model effectively
459 constrained VOD and surface soil moisture (the two retrieved variables that directly affect

460 brightness temperature), as shown in Fig. 5. Improved accuracy of the HOURLY posterior
461 relative to the prior was evident in the overall mean value of the variables, their seasonal cycles,
462 and their diurnal cycles. This success in model-data fusion occurred even though the "true
463 model" VOD and surface soil moisture were far on the lower end of the prior distributions of
464 those variables. (Note that the prior distribution was not directly specified in terms of VOD or
465 soil moisture, but rather in terms of the underlying model parameters that generate those time
466 series.) The relative difference in errors between the prior and the retrieval was much greater for
467 VOD and surface soil moisture than it was for brightness temperature, because brightness
468 temperature is also affected by the canopy and soil temperatures, which we treated as being
469 known with perfect accuracy within the OSSE.

470 3.2 Parameter retrievals

471 The HOURLY observation scenario showed the best parameter retrieval accuracy for
472 several soil parameters, one xylem parameter, and for most of the radiative transfer parameters,
473 but not for other parameters (Fig. 6). Parameters retrieved relatively accurately in all four
474 observation scenarios include the scattering albedo ω and the xylem PLC curve parameter $P63_x$.
475 All four scenarios retrieved the total soil depth Z without much bias but with large uncertainty
476 relative to the prior. For the three soil hydraulic parameters (Van Genuchten n, reference soil
477 water potential ψ_{ref}, and soil saturated hydraulic conductivity k_{soil}), each was retrieved quite
478 accurately in the HOURLY scenario, but had biases in the other scenarios. A similar pattern
479 across scenarios was found with the VOD model parameters (a, b, and c) and the maximum plant
480 water storage V. For the soil boundary condition s_{lower} and the rooting depth parameter α_{root}, the 1
481 AM/PM scenario had a large bias while the other scenarios were more accurate. For the xylem
482 conductance k_{plant}, the HOURLY scenario was most accurate, with the 1+6 scenario having a
483 bias and the two twice-daily scenarios having a larger bias. All observation scenarios exhibited
484 biases in retrievals of the stomatal parameters V_{cmax} and $P63_\beta$. This was to be expected due to our
485 imposing the Ball-Berry stomatal model on the retrieval algorithm, in contrast to the Medlyn
486 model used to generate the "true" data.
487

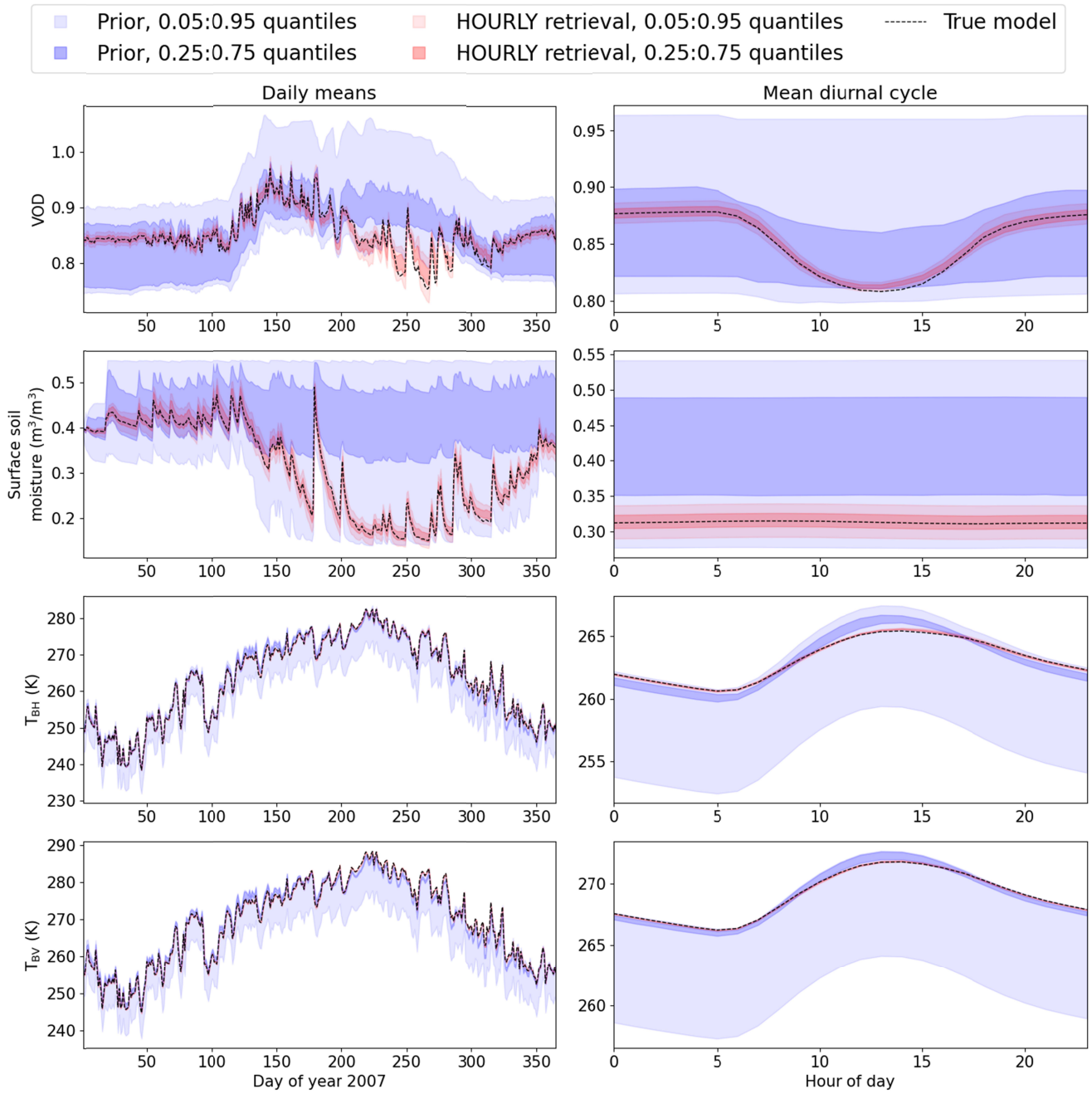

Figure 5. Comparison of VOD, surface soil moisture, and horizontally and vertically polarized brightness temperature between the prior distribution, the HOURLY retrieval posterior distribution, and the true model. For the prior and posterior distributions, the light shading represents the 0.05 to 0.95 quantile range, and the darker shading represents the 0.25 to 0.75 quantile range. Note that the "true model" brightness temperature data includes added random noise.

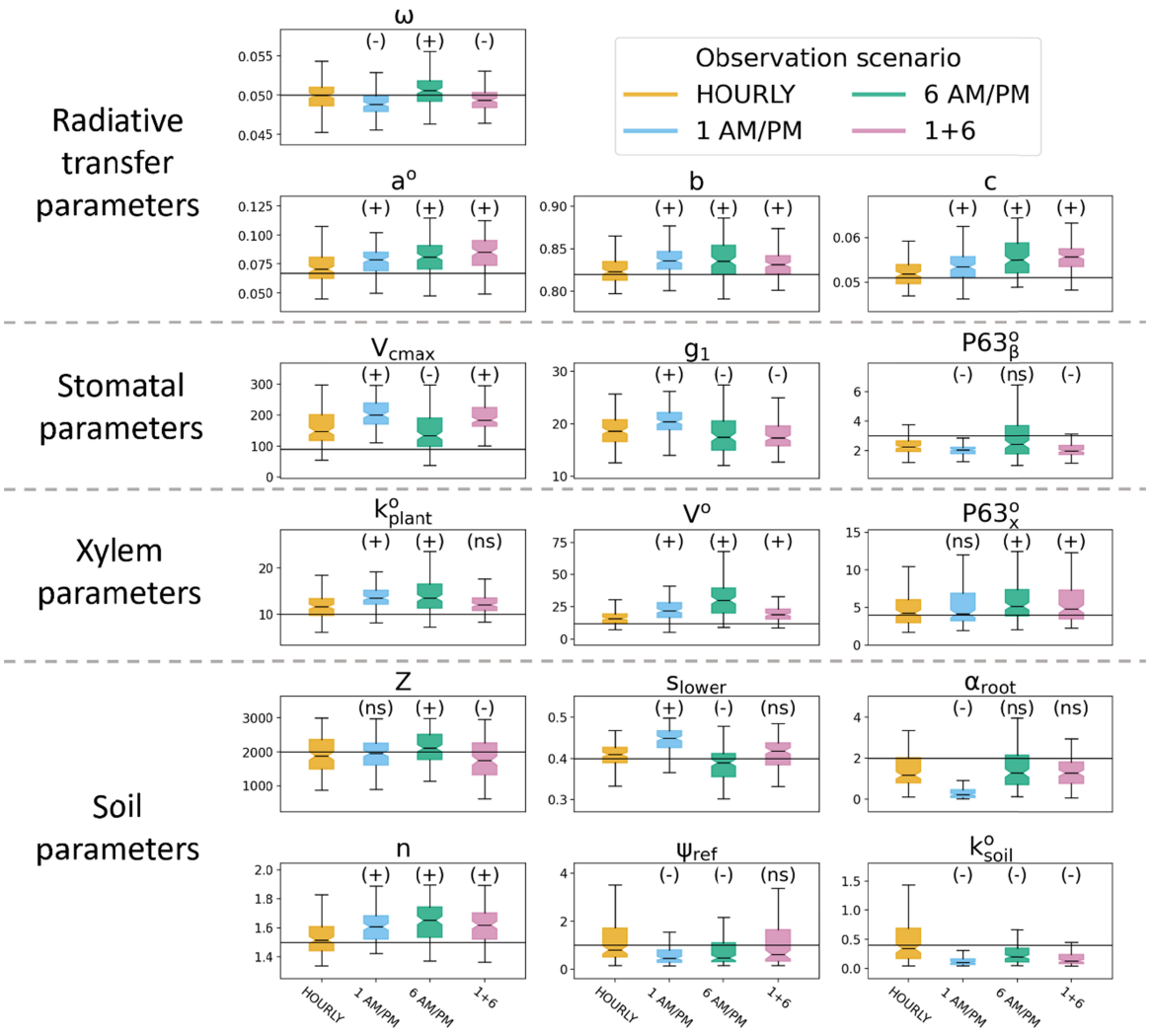

Figure 6. Posterior distributions of retrieved parameters under four observing scenarios. For each sub-panel, the black horizontal line is the "true" value, except for g_1, which does not have a "true" value because the retrievals use a different stomatal model from the "true" model run. See Table 1 for the units of each parameter. Parameters with names marked with a superscript "o" have been normalized by the value of ψ_{ref}, as described in Sect. S4. The symbols in parenthesis above the individual boxes represent statistical significance of the differences between scenarios, calculated with a Mann-Whitney U test using the HOURLY scenario as a baseline. A "(+)" mark represents significantly higher parameter values compared to the "hourly" scenario; a "(-)" mark represents significantly lower parameter values (i.e. better performance); a "(ns)" mark represents no significant difference ($p > 0.05$).

3.2 Accuracy of retrieved fluxes and water states

Over the 13-year evaluation period, the HOURLY scenario was significantly more accurate in terms of daily-mean ψ_l than the two twice-daily scenarios are, but significantly less accurate than the 1+6 scenario (Fig. 7a). A similar pattern held for ET (Fig. 7c). The fact that the 1+6 scenario was *more* accurate for ψ_l and ET than the HOURLY scenario (despite having less data) suggests that the hourly observations contained times of day where brightness temperature is not informative of plant hydraulics. Since the likelihood calculations in each scenario were normalized by the number of observations, the addition of these superfluous times of day apparently hurt the overall accuracy of the HOURLY scenario.

For column-averaged soil moisture, the HOURLY scenario was significantly more accurate than the other scenarios (Fig. 7b). This finding highlights the potential for diurnal observations to improve our estimation of multiple land surface variables, even those like soil moisture that do not change much over a single day themselves, but are influenced by variables like ET that *do* exhibit strong diurnal variation. Finally, for GPP, the twice-daily scenarios were significantly less accurate than the hourly one, while the 1+6 scenario has similar accuracy to the HOURLY one (Fig. 7d). Similar patterns of RMSE differences between observation scenarios were found when we calculated RMSE based on hourly model outputs instead of daily averages (Fig. S3).

The qualitative pattern of differences between observation scenarios over the driest summers was similar to the pattern over the entire 13-year period (Fig. 8). However, between-scenario differences in ET and GPP accuracy were larger in magnitude over these driest summers than over the entire 13-year period. Over the 13-year evaluation period, the posterior median RMSE of ET was 45% greater for the 1 AM/PM (worst) scenario than for the 1+6 scenario, while over the four driest summers the corresponding difference was 91%. Similarly for GPP, over the 13-year evaluation period, the posterior median RMSE was 21% greater for the 6 AM/PM (worst) scenario than for the 1+6 scenario, while over the four driest summers the corresponding difference was 77%.

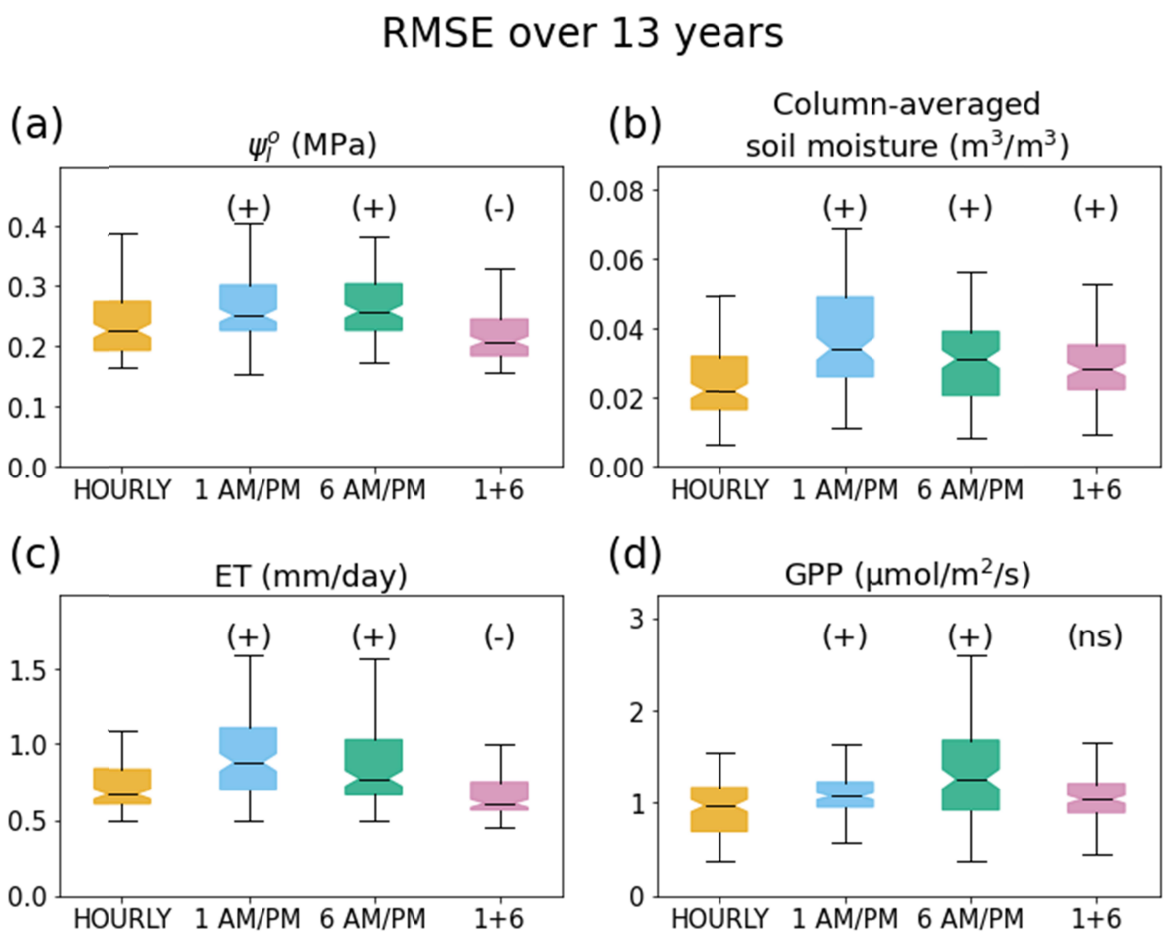

Figure 7. Box plots showing posterior distributions of RMSE for daily-averaged variables over entire evaluation period: a) normalized leaf water potential, b) column-averaged soil moisture, c) ET, d) GPP. Note that leaf water potential is normalized with respect to the soil water retention curve, as discussed in Sect. S4. The symbols in parenthesis above the individual boxes represent statistical significance of the differences between scenarios, calculated with a Mann-Whitney U test using the HOURLY scenario as a baseline. A "(+)" mark represents significantly *greater* RMSE (i.e. worse model performance) compared to the "hourly" scenario; a "(-)" mark represents significantly *smaller* RMSE (i.e. better performance); a "(ns)" mark represents no significant difference in RMSE ($p > 0.05$).

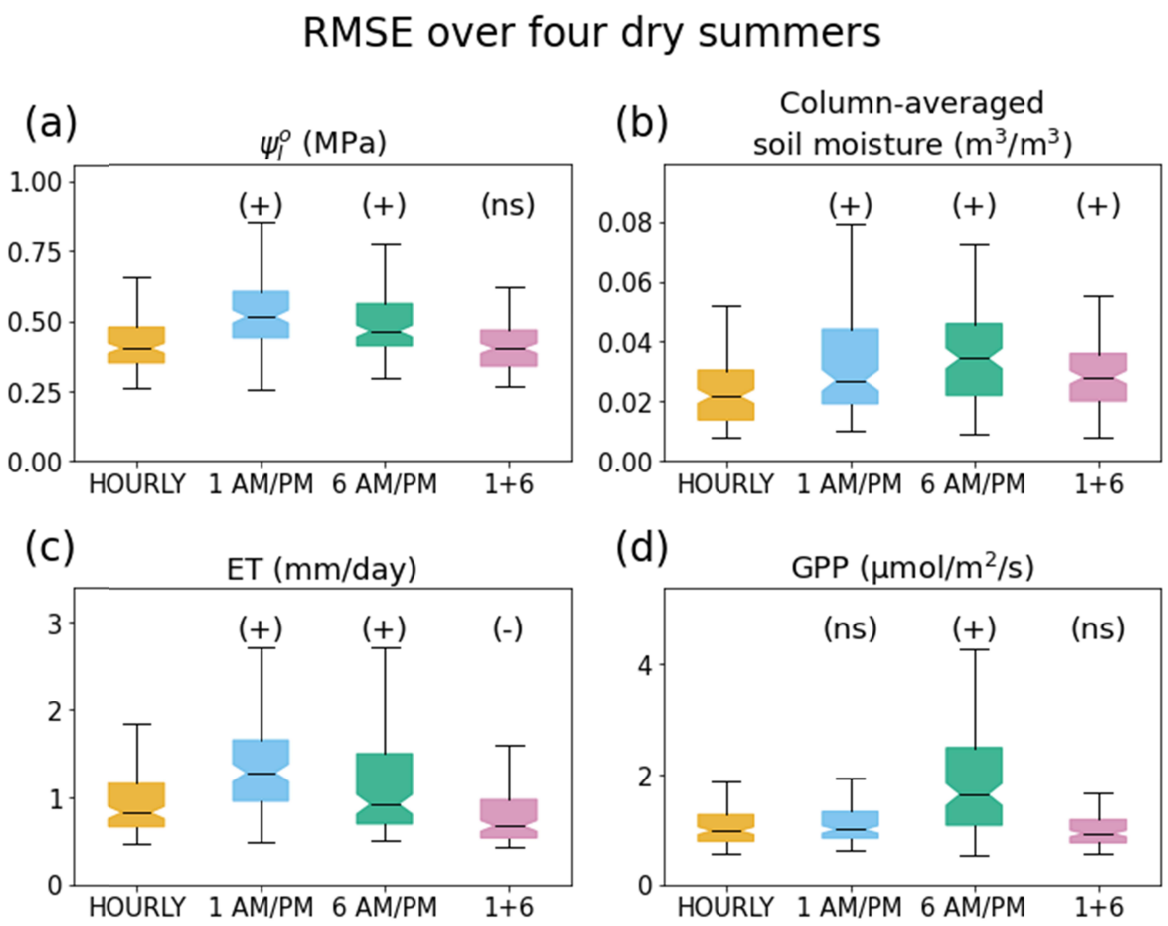

Figure 8. Box plots showing posterior distributions of RMSE for 4 daily-averaged variables over the four summers with the least precipitation. Note that leaf water potential is normalized with respect to the soil water retention curve, as discussed in Sect. S4. The symbols in parenthesis above the individual boxes represent statistical significance of the differences between scenarios, calculated with a Mann-Whitney U test using the HOURLY scenario as a baseline. A "(+)" mark represents significantly *greater* RMSE (i.e. worse model performance) compared to the "hourly" scenario; a "(-)" mark represents significantly *smaller* RMSE (i.e. better performance); a "(ns)" mark represents no significant difference in RMSE ($p > 0.05$).

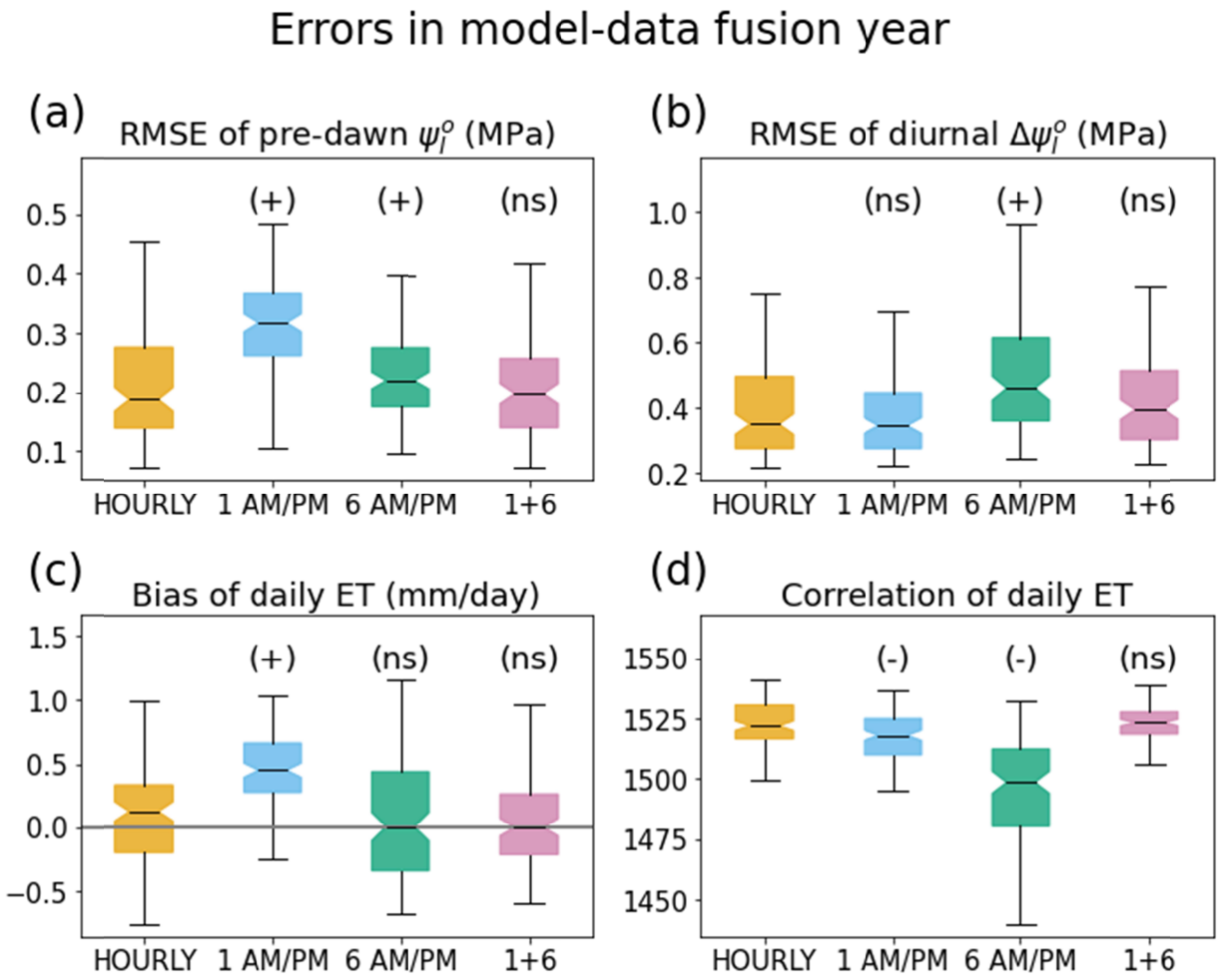

Figure 9. Box plots showing posterior distributions of several error metrics during the model-data fusion year (2007): a) RMSE of 5 AM normalized leaf water potential, b) RMSE of the diurnal amplitude of normalized leaf water potential (5 AM minus 2 PM), c) bias of daily ET, d), correlation of daily ET. Note that leaf water potential is normalized with respect to the soil water retention curve, as discussed in Sect. S4. The symbols in parenthesis above the individual boxes represent statistical significance of the differences between scenarios, calculated with a Mann-Whitney U test using the HOURLY scenario as a baseline. A "(+)" mark represents significantly greater RMSE (i.e. worse model performance) compared to the "hourly" scenario; a "(-)" mark represents significantly smaller RMSE (i.e. better performance); a "(ns)" mark represents no significant difference in RMSE ($p > 0.05$).

3.3 Drivers of differences between observational scenarios

To examine the reasons why some observation scenarios perform better than others, we broke down ψ_l errors into the RMSE of predawn ψ_l (specifically 5 AM) and the RMSE of ψ_l diurnal amplitude (Fig. 9a,b). We also calculated additional error metrics for ET: bias and Pearson correlation (Fig. 9c,d). This analysis was performed only over the model-data fusion year (2007). If we considered the entire 13-year evaluation period, it would be more likely that errors in one variable would "spill over" into other variables, leading to uncertainty over which variable is the root cause of inaccuracy.

The 1 AM/PM scenario was by far the least accurate at retrieving pre-dawn leaf water potential (Fig. 9a). This failure was presumably due to lack of observations during the predawn period when the soil and vegetation are closest to hydraulic equilibrium. The 1 AM/PM scenario thus could not constrain root-zone dynamics, and retrieved an inaccurately deep rooting depth (smaller α_{root}), with considerably greater error than in the other scenarios (Fig. 6). Due to this failure, the 1 AM/PM scenario predicted significantly higher ET than the true model (Fig. 9c) and had the largest RMSE in column-averaged soil moisture among the four scenarios (Fig. 7b).

By contrast, the 6 AM/PM scenario did especially poorly at capturing the diurnal amplitude of leaf water potential (Fig. 9c). (Here, diurnal amplitude was calculated as the difference of the 5 AM value minus the 2 PM value, where we assume based on an average diurnal cycle that 5 AM is near the diurnal maximum and 2 PM is near the diurnal minimum.) This inaccuracy may be explained by the fact that the 6 AM/PM scenario did not contain observations during the midday peak of water stress. The 6 AM/PM scenario also had the lowest Pearson correlation with the "true" ET, indicating that the 6 AM/PM retrieval did not model the temporal dynamics of ET correctly. This failure may be due to inaccurate representation of water stress and stomatal closure, resulting from the lack of observations during water-stressed hours. The $P63_\beta$ parameter (which regulates under what conditions water stress occurs) was less tightly constrained in the 6 AM/PM retrieval than in other retrievals (Fig. 6). The 6 AM/PM scenario's inaccuracy in predicting GPP (Fig. 7d) may also be related to its lack of observations of the midday period when GPP is highest within a day.

Combining 1 AM/PM observations and 6 AM/PM observations remedied the above issues with both individual observational scenarios. The 1+6 scenario predicted ET, GPP, and soil moisture significantly more accurately than in either twice-daily scenario alone (Fig. 7b-d, 8b-d, and 9c-d). This finding is not surprising, given that the 1+6 scenario is based on more observations. Our more important finding is that the 1+6 scenario has similar accuracy to the HOURLY scenario.

4 Discussion and Conclusions

4.1 Prospects for constraining plant water stress response from remote sensing

The observing scenarios analogous to a sun-synchronous orbit, with two observations per day every three days, provide a significantly worse constraint on modeled states and fluxes relative to the "geostationary" or "HOURLY" scenario. As discussed in Sect. 3.3, the two twice-daily scenarios perform poorly for different reasons related to their specific overpass times. However, combining observations from both of the sun-synchronous orbits (6 AM/PM and 1 AM/PM) constrained the model fluxes with similar accuracy to the HOURLY scenario. It appears that, at least in our case study, the complete diurnal time series of ψ_l can be inferred with

reasonable accuracy from snapshots of brightness temperature at four adequately-spaced times of day, but not from just two times of day. Consistent with these variations, the vegetation capacitance was well constrained in the HOURLY and 1+6 scenarios, but not in the 1AM/PM and 6AM/PM. Capacitance affects the shape of the VWC diurnal cycle (for example, how quickly the xylem refills at night), which may explain why more frequent sub-daily observations improve capacitance constraints. By contrast, the plant-hydraulic model data fusion study of Liu et al. (2021) found only limited ability to constrain vegetation capacitance with sun-synchronous observations from AMSR-2 alone.

In our study, model-data-fusion enhances modeled root-zone soil moisture accuracy, providing support for the idea that remote sensing of VWC could provide increased understanding of root-zone soil conditions. When sampling from the prior parameter distributions without any data constraints, the median RMSE of column-averaged soil moisture is 0.093 m^3/m^3 (not shown). The corresponding value even for the worst-performing model-data-fusion scenario (1 AM/PM) is 0.034 m^3/m^3 – a 2.7x decrease in error. This improvement occurs even though the soil parameters were less tightly constrained relative to their priors than the plant hydraulic parameters (Fig. 5). In the future, additional simulation experiments could be performed to distinguish how much of this improvement is due to brightness temperatures' sensitivity to surface soil moisture or to vegetation water content.

4.2 Retrieval accuracy is on par with that of other land surface data assimilation efforts

To put the results of our OSSE in a broader context, we can compare the errors in model states and fluxes we found here with error metrics in other studies where remote sensing or site-level data was used to constrain a land surface model. It should be expected that our study will have lower errors than comparisons with observational data, since the only sources of differences between "true" and retrieved data in our study are the noise in brightness temperatures and the intentionally incorrect stomatal conductance scheme. Assimilation studies using observational data contain additional model structural errors, inaccuracies in the forcing data such as precipitation and radiation, and potentially scaling errors between remotely sensed data and in-situ data. However, the comparison can at least provide a qualitative perspective on how much error is due to observational noise (the primary source of error simulated here) relative to other sources or inaccuracy. Here, we compare error metrics for two variables in our study with two observational data assimilation studies: Reichle et al. (2017) for root-zone soil moisture and Wang et al. (2021) for ET.

Reichle et al. (2017) compared the SMAP L4 root zone soil moisture product with in-situ measurements in the United States. The SMAP L4 product is derived by assimilating SMAP brightness temperatures into the Catchment land surface model using an ensemble Kalman filter instead of the Bayesian model-data-fusion method used here. For root zone moisture, that study found unbiased RMSE (ubRMSE, found by removing additive bias before calculating RMSE) values of approximately 0.025 to 0.03 m^3/m^3 and correlations (R) of 0.7 to 0.85. In our study, column-averaged soil moisture ubRMSE ranged between 0.015 and 0.028 m^3/m^3 for the four observing scenarios and R ranged between 0.91 and 0.97. (These metrics are calculated at a 3-hour time resolution to match the SMAP L4 study). The approximate similarity in soil moisture error ubRMSE between our study and the SMAP L4 product provides some confidence that our study realistically represents data assimilation of passive microwave remote sensing of soil moisture. Our substantially higher R values are probably a result of our experiment using the same forcing data for the "true" model and retrievals.

Wang et al. (2021) calibrated the CliMA model (without the modifications discussed in Sect. 2.2) to match measured ET and net ecosystem exchange (NEE) at the MOFLUX site. Their best-performing model setup had a mean absolute standardized error (MASE) of 29% for half-hourly ET during the growing season. MASE is calculated by dividing mean absolute error by the standard deviation of the observed or "true" data. In our study, the median growing-season MASE of hourly ET for each of the five observation scenarios relative to the "true model" ranged from 15% to 25% across scenarios. The similarity in MASE between our simulation study and Wang et al.'s real-data comparison builds additional confidence that our simulations remain close to what might be expected in a true observational scenario, despite the various idealizing assumptions.

4.3 Limitations of this study

Several assumptions and simplifications in our methodology should be acknowledged. First, our entire study is based on one site and one set of "true" parameters. A follow-up study could extend our approach to multiple sites with different plant functional types and climatic conditions, and/or include multiple values of prescribed "true" parameters to retrieve. Second, we only tested one assumption about which plant components contribute to VOD (leaves, but not branches or stems). The relative contributions of different plant components to VOD may differ by wavelength and by plant type (Ferrazzoli & Guerriero, 1996). Additionally, since VOD measures total canopy water, it be affected by water on the surface of leaves (canopy interception and dew), which is not currently considered in the CliMA model. Studies that have examined the effect of this canopy surface water on microwave remote sensing observables have variously found large effects (Khabbazan et al., 2022; X. Xu et al., 2021), small and potentially negligeable effects (Hornbuckle et al., 2007), or no measurable effect (Escorihuela et al., 2009; Holtzman et al., 2021). Whether canopy surface water can be ignored while studying VOD presumably depends on local conditions including leaf area and canopy structure (smaller leaves would intercept less water), and how often meteorological conditions favorable for dew occur.

We did not explore the full possible spectrum of complexity in the radiative transfer model. First, we assumed a particular and relatively simple relationship between leaf water potential, VWC, and VOD. More physically detailed parametrizations of the VWC-VOD relationship have recently been proposed (Fink et al., 2018; Humphrey & Frankenberg, 2022), as well as alternative empirical models to Eqn. 1 (Forkel et al., 2023). Second, we treated the VOD model coefficients (*a, b,* and *c*) and the scattering albedo ω as constant over time. However, in many ecosystems the scattering albedo van vary significantly over time with seasonal and interannual changes in vegetation structure (Baur et al., 2021; Konings et al., 2016; H. Wang et al., 2023). Third, we treated the effect of soil roughness on brightness temperature at our site as known a priori, when it varies spatially. Pixel-wise tuning of the roughness parametrization has been shown to reduce radiative transfer model biases in the context of passive microwave data assimilation (Lievens et al., 2015). A more realistic treatment of the roughness parametrization would also vary in time, since the roughness parametrization implicitly accounts for leaf litter, which interacts differently with microwaves when the litter is wet (after rainfall) from when it is dry (Kurum et al., 2012; Wigneron et al., 2017). Finally, the tau-omega radiative transfer model we used does not account for multiple scattering by vegetation, which can lead to errors when used in very dense forests where more complicated radiative transfer models are more appropriate (Ambadan et al., 2022; Feldman, Akbar, et al., 2018)

Another simplification we made was our assumption of perfect knowledge of soil and canopy temperatures throughout the day (these physical temperatures are used in relating VOD and surface soil moisture to microwave brightness temperatures). Future versions of the CliMA model will have prognostic soil and canopy temperatures, which would allow brightness temperature to be used as a constraint without requiring external soil/canopy temperature data, as is done in other land surface models (Han et al., 2014; Reichle et al., 2017). One challenge with this approach is that the difference between air and canopy temperatures is highly variable by time of day and vegetation type (Javadian et al., 2022; Still et al., 2022).

Remotely sensed land surface temperature itself is available at high temporal resolution from geostationary satellites such as GOES and the Spinning Enhanced Visible and Infrared Imager (SEVIRI) (Sun & Pinker, 2003; Y. Yu et al., 2012). The combination of LST and microwave brightness temperature can be used to jointly constrain a land surface model (Lu et al., 2017). It is possible that some of the benefit of frequent microwave observations found in our study could also be realized from combining twice-daily microwave data with hourly LST. Simultaneously assimilating additional forms of remote sensing data might also be useful, such as solar induced fluorescence (SIF) which is linked to photosynthesis and thus GPP (Norton et al., 2019).

4.4 Implications for satellite missions

Our findings are encouraging for efforts to estimate ecosystem carbon and water fluxes and plant hydraulic traits by fusing existing satellite data with plant hydraulics-enabled land surface models (with the caveat that vegetation trait values retrieved from model-data fusion are specific to the land surface model used). Based on the good performance of the four-times-daily scenario, combining data from multiple microwave satellites, with overpass times covering both pre-dawn and mid-day, should be beneficial to model-data-fusion efforts. This finding has implications for planning future satellite missions. It may also be possible to realize the benefits of such an approach by combining datasets from multiple currently operating missions. However, in that case there are additional challenges. Post-processing and careful uncertainty analysis would be required to co-locate the data from sensors with different spatial resolutions onto a common grid. Also, sensors operating in different wavelengths typically have differing effective penetration depths through the canopy, so the effect of vegetation water content on VOD differs by sensor, necessitating a separate observation operator for each sensor in the model-data-fusion process. These factors were not considered in our study, where we assumed the 6 AM/PM and 1 AM/PM overpasses interacted with the vegetation in identical ways. Nevertheless, if between-sensor differences can be accounted for, using data from both SMAP and AMSR2 as a constraint, for example, should provide a significant boost in trait accuracy and modeled fluxes compared to only using observations from one microwave sensor.

Acknowledgments

NH is supported by a Future Investigators in NASA Earth and Space Science and Technology (FINESST) grant (80NSSC20K1620) from the National Aeronautics and Space Administration (NASA). NH, AGK, JDW, and CF are supported by the NASA Carbon Cycle Science program (80NSSC21K1712). NH and AGK are also supported by NSF DEB-1942133.

YW and CF gratefully acknowledge the generous support of Eric and Wendy Schmidt (by recommendation of the Schmidt Futures initiative) and the Heising-Simons Foundation.

Open Research

All code used in this project is available in a GitHub repository:

https://github.com/natan-holtzman/CliMa_Microwave

The repository includes source code for our version of the CliMA Land model, meteorological data used as model forcing, MCMC code for the retrieval algorithm, and scripts to analyze the model outputs and produce the figures in this paper.

The following Zenodo repository contains retrieved posterior parameter distributions, and posterior quantiles for the retrieved time series of model states and fluxes:

https://doi.org/10.5281/zenodo.7757684

References

Ambadan, J. T., MacRae, H. C., Colliander, A., Tetlock, E., Helgason, W., Gedalof, Z., & Berg, A. A. (2022). Evaluation of SMAP Soil Moisture Retrieval Accuracy Over a Boreal Forest Region. *IEEE Transactions on Geoscience and Remote Sensing*, *60*, 1–11. https://doi.org/10.1109/TGRS.2022.3212934

Anderegg, W. R. L. (2015). Spatial and temporal variation in plant hydraulic traits and their relevance for climate change impacts on vegetation. *New Phytologist*, *205*(3), Article 3. https://doi.org/10.1111/nph.12907

Arnold, C. P., & Dey, C. H. (1986). Observing-Systems Simulation Experiments: Past, Present, and Future. *Bulletin of the American Meteorological Society*, *67*(6), 687–695. https://doi.org/10.1175/1520-0477(1986)067<0687:OSSEPP>2.0.CO;2

Atlas, R. (1997). Atmospheric Observations and Experiments to Assess Their Usefulness in Data Assimilation (gtSpecial IssueltData Assimilation in Meteology and Oceanography:

779 Theory and Practice). *Journal of the Meteorological Society of Japan. Ser. II*, *75*(1B),
780 111–130. https://doi.org/10.2151/jmsj1965.75.1B_111
781 Ball, J. T., Woodrow, I. E., & Berry, J. A. (1987). A Model Predicting Stomatal Conductance
782 and its Contribution to the Control of Photosynthesis under Different Environmental
783 Conditions. In J. Biggins (Ed.), *Progress in Photosynthesis Research* (pp. 221–224).
784 Springer Netherlands. https://doi.org/10.1007/978-94-017-0519-6_48
785 Baur, M. J., Jagdhuber, T., Feldman, A. F., Chaparro, D., Piles, M., & Entekhabi, D. (2021).
786 Time-variations of zeroth-order vegetation absorption and scattering at L-band. *Remote*
787 *Sensing of Environment*, *267*, 112726. https://doi.org/10.1016/j.rse.2021.112726
788 Chan, S. K., Bindlish, R., O'Neill, P. E., Njoku, E., Jackson, T., Colliander, A., Chen, F., Burgin,
789 M., Dunbar, S., Piepmeier, J., Yueh, S., Entekhabi, D., Cosh, M. H., Caldwell, T.,
790 Walker, J., Wu, X., Berg, A., Rowlandson, T., Pacheco, A., … Kerr, Y. (2016).
791 Assessment of the SMAP Passive Soil Moisture Product. *IEEE Transactions on*
792 *Geoscience and Remote Sensing*, *54*(8), Article 8.
793 https://doi.org/10.1109/TGRS.2016.2561938
794 De Lannoy, G. J. M., & Reichle, R. H. (2016). Global Assimilation of Multiangle and
795 Multipolarization SMOS Brightness Temperature Observations into the GEOS-5
796 Catchment Land Surface Model for Soil Moisture Estimation. *Journal of*
797 *Hydrometeorology*, *17*(2), 669–691. https://doi.org/10.1175/JHM-D-15-0037.1
798 Ding, Y., Nie, Y., Chen, H., Wang, K., & Querejeta, J. I. (2021). Water uptake depth is
799 coordinated with leaf water potential, water-use efficiency and drought vulnerability in
800 karst vegetation. *New Phytologist*, *229*(3), 1339–1353. https://doi.org/10.1111/nph.16971

Eller, C. B., Rowland, L., Mencuccini, M., Rosas, T., Williams, K., Harper, A., Medlyn, B. E., Wagner, Y., Klein, T., Teodoro, G. S., Oliveira, R. S., Matos, I. S., Rosado, B. H. P., Fuchs, K., Wohlfahrt, G., Montagnani, L., Meir, P., Sitch, S., & Cox, P. M. (2020). Stomatal optimization based on xylem hydraulics (SOX) improves land surface model simulation of vegetation responses to climate. *New Phytologist*, *226*(6), 1622–1637. https://doi.org/10.1111/nph.16419

Entekhabi, D., Njoku, E. G., O'Neill, P. E., Kellogg, K. H., Crow, W. T., Edelstein, W. N., Entin, J. K., Goodman, S. D., Jackson, T. J., Johnson, J., Kimball, J., Piepmeier, J. R., Koster, R. D., Martin, N., McDonald, K. C., Moghaddam, M., Moran, S., Reichle, R., Shi, J. C., … Van Zyl, J. (2010). The Soil Moisture Active Passive (SMAP) Mission. *Proceedings of the IEEE*, *98*(5), Article 5. https://doi.org/10.1109/JPROC.2010.2043918

Escorihuela, M. J., Kerr, Y. H., de Rosnay, P., Saleh, K., Wigneron, J.-P., & Calvet, J. C. (2009). Effects of Dew on the Radiometric Signal of a Grass Field at L-Band. *IEEE Geoscience and Remote Sensing Letters*, *6*(1), Article 1. https://doi.org/10.1109/LGRS.2008.2000714

Farquhar, G. D., von Caemmerer, S., & Berry, J. A. (1980). A biochemical model of photosynthetic CO2 assimilation in leaves of C3 species. *Planta*, *149*(1), 78–90. https://doi.org/10.1007/BF00386231

Feldman, A. F., Akbar, R., & Entekhabi, D. (2018). Characterization of higher-order scattering from vegetation with SMAP measurements. *Remote Sensing of Environment*, *219*, 324–338. https://doi.org/10.1016/j.rse.2018.10.022

Feldman, A. F., Short Gianotti, D. J., Konings, A. G., Gentine, P., & Entekhabi, D. (2021). Patterns of plant rehydration and growth following pulses of soil moisture availability. *Biogeosciences*, *18*(3), Article 3. https://doi.org/10.5194/bg-18-831-2021

824 Feldman, A. F., Short Gianotti, D. J., Konings, A. G., McColl, K. A., Akbar, R., Salvucci, G. D.,
825 & Entekhabi, D. (2018). Moisture pulse-reserve in the soil-plant continuum observed
826 across biomes. *Nature Plants*, *4*(12), 1026–1033. https://doi.org/10.1038/s41477-018-
827 0304-9
828 Feldman, A. F., Short Gianotti, D. J., Trigo, I. F., Salvucci, G. D., & Entekhabi, D. (2020). Land-
829 Atmosphere Drivers of Landscape-Scale Plant Water Content Loss. *Geophysical*
830 *Research Letters*, *47*(22). https://doi.org/10.1029/2020GL090331
831 Ferrazzoli, P., & Guerriero, L. (1996). Passive microwave remote sensing of forests: A model
832 investigation. *IEEE Transactions on Geoscience and Remote Sensing*, *34*(2), Article 2.
833 https://doi.org/10.1109/36.485121
834 Fink, A., Jagdhuber, T., Piles, M., Grant, J., Baur, M., Link, M., & Entekhabi, D. (2018).
835 Estimating Gravimetric Moisture of Vegetation Using an Attenuation-Based Multi-
836 Sensor Approach. *IGARSS 2018 - 2018 IEEE International Geoscience and Remote*
837 *Sensing Symposium*, 353–356. https://doi.org/10.1109/IGARSS.2018.8518949
838 Forkel, M., Schmidt, L., Zotta, R.-M., Dorigo, W., & Yebra, M. (2023). Estimating leaf moisture
839 content at global scale from passive microwave satellite observations of vegetation
840 optical depth. *Hydrology and Earth System Sciences*, *27*(1), 39–68.
841 https://doi.org/10.5194/hess-27-39-2023
842 Frank, D., Reichstein, M., Bahn, M., Thonicke, K., Frank, D., Mahecha, M. D., Smith, P., Velde,
843 M., Vicca, S., Babst, F., Beer, C., Buchmann, N., Canadell, J. G., Ciais, P., Cramer, W.,
844 Ibrom, A., Miglietta, F., Poulter, B., Rammig, A., … Zscheischler, J. (2015). Effects of
845 climate extremes on the terrestrial carbon cycle: Concepts, processes and potential future
846 impacts. *Global Change Biology*, *21*(8), 2861–2880. https://doi.org/10.1111/gcb.12916

Gelman, A., & Rubin, D. B. (1992). Inference from Iterative Simulation Using Multiple Sequences. *Statistical Science*, *7*(4). https://doi.org/10.1214/ss/1177011136

Gu, L., Pallardy, S. G., Yang, B., Hosman, K. P., Mao, J., Ricciuto, D., Shi, X., & Sun, Y. (2016). Testing a land model in ecosystem functional space via a comparison of observed and modeled ecosystem flux responses to precipitation regimes and associated stresses in a Central U.S. forest. *Journal of Geophysical Research: Biogeosciences*, *121*(7), 1884–1902. https://doi.org/10.1002/2015JG003302

Haario, H., Saksman, E., & Tamminen, J. (2001). An adaptive Metropolis algorithm. *Bernoulli*, *7*(2), Article 2.

Han, X., Franssen, H.-J. H., Montzka, C., & Vereecken, H. (2014). Soil moisture and soil properties estimation in the Community Land Model with synthetic brightness temperature observations. *Water Resources Research*, *50*(7), 6081–6105. https://doi.org/10.1002/2013WR014586

Holtzman, N. M., Anderegg, L. D. L., Kraatz, S., Mavrovic, A., Sonnentag, O., Pappas, C., Cosh, M. H., Langlois, A., Lakhankar, T., Tesser, D., Steiner, N., Colliander, A., Roy, A., & Konings, A. G. (2021). L-band vegetation optical depth as an indicator of plant water potential in a temperate deciduous forest stand. *Biogeosciences*, *18*(2), 739–753. https://doi.org/10.5194/bg-18-739-2021

Hornbuckle, B. K., England, A. W., & Anderson, M. C. (2007). The Effect of Intercepted Precipitation on the Microwave Emission of Maize at 1.4 GHz. *IEEE Transactions on Geoscience and Remote Sensing*, *45*(7), 1988–1995. https://doi.org/10.1109/TGRS.2007.894057

869 Humphrey, V., & Frankenberg, C. (2022). *Continuous ground monitoring of vegetation optical*
870 *depth and water content with GPS signals* [Preprint]. Biogeophysics: Ecohydrology.
871 https://doi.org/10.5194/bg-2022-84
872 Jackson, T. J., & Schmugge, T. J. (1991). Vegetation effects on the microwave emission of soils.
873 *Remote Sensing of Environment*, *36*(3), 203–212. https://doi.org/10.1016/0034-
874 4257(91)90057-D
875 Javadian, M., Smith, W. K., Lee, K., Knowles, J. F., Scott, R. L., Fisher, J. B., Moore, D. J. P.,
876 Leeuwen, W. J. D., Barron-Gafford, G., & Behrangi, A. (2022). Canopy Temperature Is
877 Regulated by Ecosystem Structural Traits and Captures the Ecohydrologic Dynamics of a
878 Semiarid Mixed Conifer Forest Site. *Journal of Geophysical Research: Biogeosciences*,
879 *127*(2). https://doi.org/10.1029/2021JG006617
880 Kachi, M., Hori, M., Maeda, T., & Imaoka, K. (2014). Status of validation of AMSR2 on board
881 the GCOM-W1 satellite. *2014 IEEE Geoscience and Remote Sensing Symposium*, 110–
882 113. https://doi.org/10.1109/IGARSS.2014.6946368
883 Katerji, N., Hallaire, M., Menoux-Boyer, Y., & Durand, B. (1986). Modelling diurnal patterns of
884 leaf water potential in field conditions. *Ecological Modelling*, *33*(2–4), 185–203.
885 https://doi.org/10.1016/0304-3800(86)90040-2
886 Kennedy, D., Swenson, S., Oleson, K. W., Lawrence, D. M., Fisher, R., Lola da Costa, A. C., &
887 Gentine, P. (2019). Implementing Plant Hydraulics in the Community Land Model,
888 Version 5. *Journal of Advances in Modeling Earth Systems*, *11*(2), 485–513.
889 https://doi.org/10.1029/2018MS001500
890 Khabbazan, S., Steele-Dunne, S. C., Vermunt, P., Judge, J., Vreugdenhil, M., & Gao, G. (2022).
891 The influence of surface canopy water on the relationship between L-band backscatter

892 and biophysical variables in agricultural monitoring. *Remote Sensing of Environment*,
893 *268*, 112789. https://doi.org/10.1016/j.rse.2021.112789
894 Khan, A. M., Stoy, P. C., Douglas, J. T., Anderson, M., Diak, G., Otkin, J. A., Hain, C., Rehbein,
895 E. M., & McCorkel, J. (2021). Reviews and syntheses: Ongoing and emerging
896 opportunities to improve environmental science using observations from the Advanced
897 Baseline Imager on the Geostationary Operational Environmental Satellites.
898 *Biogeosciences*, *18*(13), 4117–4141. https://doi.org/10.5194/bg-18-4117-2021
899 Khatami, S., Peel, M. C., Peterson, T. J., & Western, A. W. (2019). Equifinality and Flux
900 Mapping: A New Approach to Model Evaluation and Process Representation Under
901 Uncertainty. *Water Resources Research*, *55*(11), 8922–8941.
902 https://doi.org/10.1029/2018WR023750
903 Kim, H., Parinussa, R., Konings, A. G., Wagner, W., Cosh, M. H., Lakshmi, V., Zohaib, M., &
904 Choi, M. (2018). Global-scale assessment and combination of SMAP with ASCAT
905 (active) and AMSR2 (passive) soil moisture products. *Remote Sensing of Environment*,
906 *204*, 260–275. https://doi.org/10.1016/j.rse.2017.10.026
907 Klein, T. (2014). The variability of stomatal sensitivity to leaf water potential across tree species
908 indicates a continuum between isohydric and anisohydric behaviours. *Functional*
909 *Ecology*, *28*(6), 1313–1320. https://doi.org/10.1111/1365-2435.12289
910 Klepper, B. (1968). Diurnal Pattern of Water Potential in Woody Plants. *Plant Physiology*,
911 *43*(12), Article 12. https://doi.org/10.1104/pp.43.12.1931
912 Konings, A. G., & Gentine, P. (2017). Global variations in ecosystem-scale isohydricity. *Global*
913 *Change Biology*, *23*(2), Article 2. https://doi.org/10.1111/gcb.13389

914 Konings, A. G., Piles, M., Das, N., & Entekhabi, D. (2017). L-band vegetation optical depth and
915 effective scattering albedo estimation from SMAP. *Remote Sensing of Environment*, *198*,
916 460–470. https://doi.org/10.1016/j.rse.2017.06.037
917 Konings, A. G., Piles, M., Rötzer, K., McColl, K. A., Chan, S. K., & Entekhabi, D. (2016).
918 Vegetation optical depth and scattering albedo retrieval using time series of dual-
919 polarized L-band radiometer observations. *Remote Sensing of Environment*, *172*, 178–
920 189. https://doi.org/10.1016/j.rse.2015.11.009
921 Konings, A. G., Rao, K., & Steele-Dunne, S. C. (2019). Macro to Micro: Microwave Remote
922 Sensing of Plant Water Content for Physiology and Ecology. *New Phytologist*.
923 https://doi.org/10.1111/nph.15808
924 Konings, A. G., Saatchi, S. S., Frankenberg, C., Keller, M., Leshyk, V., Anderegg, W. R. L.,
925 Humphrey, V., Matheny, A. M., Trugman, A., Sack, L., Agee, E., Barnes, M. L., Binks,
926 O., Cawse-Nicholson, K., Christoffersen, B. O., Entekhabi, D., Gentine, P., Holtzman, N.
927 M., Katul, G. G., … Zuidema, P. A. (2021). Detecting forest response to droughts with
928 global observations of vegetation water content. *Global Change Biology*, *27*(23), 6005–
929 6024. https://doi.org/10.1111/gcb.15872
930 Kumar, S., Holmes, T. R., Bindlish, R., de Jeu, R., & Peters-Lidard, C. (2020). Assimilation of
931 vegetation optical depth retrievals from passive microwave radiometry. *Hydrology and*
932 *Earth System Sciences*, *24*(7), Article 7. https://doi.org/10.5194/hess-24-3431-2020
933 Kumar, S., Kolassa, J., Reichle, R., Crow, W., de Lannoy, G., de Rosnay, P., MacBean, N.,
934 Girotto, M., Fox, A., Quaife, T., Draper, C., Forman, B., Balsamo, G., Steele-Dunne, S.,
935 Albergel, C., Bonan, B., Calvet, J., Dong, J., Liddy, H., & Ruston, B. (2022). An Agenda
936 for Land Data Assimilation Priorities: Realizing the Promise of Terrestrial Water,

937 Energy, and Vegetation Observations From Space. *Journal of Advances in Modeling*
938 *Earth Systems*, *14*(11). https://doi.org/10.1029/2022MS003259
939 Kurum, M., O'Neill, P. E., Lang, R. H., Cosh, M. H., Joseph, A. T., & Jackson, T. J. (2012).
940 Impact of Conifer Forest Litter on Microwave Emission at L-Band. *IEEE Transactions*
941 *on Geoscience and Remote Sensing*, *50*(4), 1071–1084.
942 https://doi.org/10.1109/TGRS.2011.2166272
943 Li, L., Yang, Z., Matheny, A. M., Zheng, H., Swenson, S. C., Lawrence, D. M., Barlage, M.,
944 Yan, B., McDowell, N. G., & Leung, L. R. (2021). Representation of Plant Hydraulics in
945 the Noah-MP Land Surface Model: Model Development and Multiscale Evaluation.
946 *Journal of Advances in Modeling Earth Systems*, *13*(4).
947 https://doi.org/10.1029/2020MS002214
948 Li, X., Wigneron, J.-P., Frappart, F., Fan, L., Ciais, P., Fensholt, R., Entekhabi, D., Brandt, M.,
949 Konings, A. G., Liu, X., Wang, M., Al-Yaari, A., & Moisy, C. (2021). Global-scale
950 assessment and inter-comparison of recently developed/reprocessed microwave satellite
951 vegetation optical depth products. *Remote Sensing of Environment*, *253*, 112208.
952 https://doi.org/10.1016/j.rse.2020.112208
953 Lievens, H., Al Bitar, A., Verhoest, N. E. C., Cabot, F., De Lannoy, G. J. M., Drusch, M.,
954 Dumedah, G., Hendricks Franssen, H.-J., Kerr, Y., Tomer, S. K., Martens, B., Merlin, O.,
955 Pan, M., van den Berg, M. J., Vereecken, H., Walker, J. P., Wood, E. F., & Pauwels, V.
956 R. N. (2015). Optimization of a Radiative Transfer Forward Operator for Simulating
957 SMOS Brightness Temperatures over the Upper Mississippi Basin. *Journal of*
958 *Hydrometeorology*, *16*(3), 1109–1134. https://doi.org/10.1175/JHM-D-14-0052.1

959 Liu, Y., Holtzman, N. M., & Konings, A. G. (2021). Global ecosystem-scale plant hydraulic
960 traits retrieved using model–data fusion. *Hydrology and Earth System Sciences*, *25*(5),
961 2399–2417. https://doi.org/10.5194/hess-25-2399-2021
962 Liu, Y., Konings, A. G., Kennedy, D., & Gentine, P. (2021). Global Coordination in Plant
963 Physiological and Rooting Strategies in Response to Water Stress. *Global*
964 *Biogeochemical Cycles*, *35*(7), Article 7. https://doi.org/10.1029/2020GB006758
965 Liu, Y., Kumar, M., Katul, G. G., Feng, X., & Konings, A. G. (2020). Plant hydraulics
966 accentuates the effect of atmospheric moisture stress on transpiration. *Nature Climate*
967 *Change*, *10*(7), Article 7. https://doi.org/10.1038/s41558-020-0781-5
968 Liu, Y., Parolari, A. J., Kumar, M., Huang, C.-W., Katul, G. G., & Porporato, A. (2017).
969 Increasing atmospheric humidity and CO2 concentration alleviate forest mortality risk.
970 *Proceedings of the National Academy of Sciences*, *114*(37), Article 37.
971 https://doi.org/10.1073/pnas.1704811114
972 Liu, Y. Y., de Jeu, R. A. M., McCabe, M. F., Evans, J. P., & van Dijk, A. I. J. M. (2011). Global
973 long-term passive microwave satellite-based retrievals of vegetation optical depth.
974 *Geophysical Research Letters*, *38*(18), Article 18. https://doi.org/10.1029/2011GL048684
975 Lu, Y., Steele-Dunne, S. C., Farhadi, L., & van de Giesen, N. (2017). Mapping Surface Heat
976 Fluxes by Assimilating SMAP Soil Moisture and GOES Land Surface Temperature Data.
977 *Water Resources Research*, *53*(12), 10858–10877.
978 https://doi.org/10.1002/2017WR021415
979 M van Genuchten. (1980). A Closed-form Equation for Predicting the Hydraulic Conductivity of
980 Unsaturated Soils. *Soil Science Society of America Journal*.

MacBean, N., Liddy, H., Quaife, T., Kolassa, J., & Fox, A. (2022). Building a Land Data Assimilation Community to Tackle Technical Challenges in Quantifying and Reducing Uncertainty in Land Model Predictions. *Bulletin of the American Meteorological Society*, *103*(3), E733–E740. https://doi.org/10.1175/BAMS-D-21-0228.1

Manzoni, S., Katul, G., & Porporato, A. (2014). A dynamical system perspective on plant hydraulic failure. *Water Resources Research*, *50*(6), 5170–5183. https://doi.org/10.1002/2013WR015236

Martinez-Vilalta, J., Anderegg, W. R. L., Sapes, G., & Sala, A. (2019). Greater focus on water pools may improve our ability to understand and anticipate drought-induced mortality in plants. *New Phytologist*, *223*(1), 22–32. https://doi.org/10.1111/nph.15644

Martin-StPaul, N., Delzon, S., & Cochard, H. (2017). Plant resistance to drought depends on timely stomatal closure. *Ecology Letters*, *20*(11), 1437–1447. https://doi.org/10.1111/ele.12851

Matheny, A. M., Bohrer, G., Stoy, P. C., Baker, I. T., Black, A. T., Desai, A. R., Dietze, M. C., Gough, C. M., Ivanov, V. Y., Jassal, R. S., Novick, K. A., Schäfer, K. V. R., & Verbeeck, H. (2014). Characterizing the diurnal patterns of errors in the prediction of evapotranspiration by several land-surface models: An NACP analysis. *Journal of Geophysical Research: Biogeosciences*, *119*(7), Article 7. https://doi.org/10.1002/2014JG002623

Matheny, A. M., Fiorella, R. P., Bohrer, G., Poulsen, C. J., Morin, T. H., Wunderlich, A., Vogel, C. S., & Curtis, P. S. (2017). Contrasting strategies of hydraulic control in two codominant temperate tree species. *Ecohydrology*, *10*(3), Article 3. https://doi.org/10.1002/eco.1815

McDowell, N., Pockman, W. T., Allen, C. D., Breshears, D. D., Cobb, N., Kolb, T., Plaut, J., Sperry, J., West, A., Williams, D. G., & Yepez, E. A. (2008). Mechanisms of plant survival and mortality during drought: Why do some plants survive while others succumb to drought? *New Phytologist*, *178*(4), 719–739. https://doi.org/10.1111/j.1469-8137.2008.02436.x

Medlyn, B. E., Duursma, R. A., Eamus, D., Ellsworth, D. S., Prentice, I. C., Barton, C. V. M., Crous, K. Y., De Angelis, P., Freeman, M., & Wingate, L. (2011). Reconciling the optimal and empirical approaches to modelling stomatal conductance. *Global Change Biology*, *17*(6), Article 6. https://doi.org/10.1111/j.1365-2486.2010.02375.x

Mirfenderesgi, G., Bohrer, G., Matheny, A. M., Fatichi, S., de Moraes Frasson, R. P., & Schäfer, K. V. R. (2016). Tree level hydrodynamic approach for resolving aboveground water storage and stomatal conductance and modeling the effects of tree hydraulic strategy: Stomatal Conductance Parameterization. *Journal of Geophysical Research: Biogeosciences*, *121*(7), 1792–1813. https://doi.org/10.1002/2016JG003467

Mironov, V. L., Dobson, M. C., Kaupp, V. H., Komarov, S. A., & Kleshchenko, V. N. (2002). Generalized refractive mixing dielectric model for moist soils. *IEEE International Geoscience and Remote Sensing Symposium*, *6*, 3556–3558. https://doi.org/10.1109/IGARSS.2002.1027247

Mo, T., Choudhury, B. J., Schmugge, T. J., Wang, J. R., & Jackson, T. J. (1982). A model for microwave emission from vegetation-covered fields. *Journal of Geophysical Research*, *87*(C13), 11229. https://doi.org/10.1029/JC087iC13p11229

Momen, M., Wood, J. D., Novick, K. A., Pangle, R., Pockman, W. T., McDowell, N. G., & Konings, A. G. (2017). Interacting Effects of Leaf Water Potential and Biomass on

1027 Vegetation Optical Depth: Effects of LWP and Biomass on VOD. *Journal of*
1028 *Geophysical Research: Biogeosciences*, *122*(11), 3031–3046.
1029 https://doi.org/10.1002/2017JG004145
1030 Munger, W., & Wofsy, S. (2020). *Biomass Inventories at Harvard Forest EMS Tower since*
1031 *1993* [Data set]. Environmental Data Initiative.
1032 https://doi.org/10.6073/PASTA/C27CDE917CCC89CA0A131525FCD328B8
1033 Myneni, R. B., Hoffman, S., Knyazikhin, Y., Privette, J. L., Glassy, J., Tian, Y., Wang, Y., Song,
1034 X., Zhang, Y., Smith, G. R., Lotsch, A., Friedl, M., Morisette, J. T., Votava, P., Nemani,
1035 R. R., & Running, S. W. (2002). Global products of vegetation leaf area and fraction
1036 absorbed PAR from year one of MODIS data. *Remote Sensing of Environment*, *83*(1–2),
1037 Article 1–2. https://doi.org/10.1016/S0034-4257(02)00074-3
1038 Nelson, J. A., Carvalhais, N., Migliavacca, M., Reichstein, M., & Jung, M. (2018). Water-stress-
1039 induced breakdown of carbon–water relations: Indicators from diurnal FLUXNET
1040 patterns. *Biogeosciences*, *15*(8), 2433–2447. https://doi.org/10.5194/bg-15-2433-2018
1041 Nolan, R. H., Boer, M. M., Resco de Dios, V., Caccamo, G., & Bradstock, R. A. (2016). Large-
1042 scale, dynamic transformations in fuel moisture drive wildfire activity across
1043 southeastern Australia: Transformations in Fuel Moisture. *Geophysical Research Letters*,
1044 *43*(9), Article 9. https://doi.org/10.1002/2016GL068614
1045 Norton, A. J., Rayner, P. J., Koffi, E. N., Scholze, M., Silver, J. D., & Wang, Y.-P. (2019).
1046 Estimating global gross primary productivity using chlorophyll fluorescence and a data
1047 assimilation system with the BETHY-SCOPE model. *Biogeosciences*, *16*(15), 3069–
1048 3093. https://doi.org/10.5194/bg-16-3069-2019

1049 Novick, K. A., Ficklin, D. L., Baldocchi, D., Davis, K. J., Ghezzehei, T. A., Konings, A. G.,
1050 MacBean, N., Raoult, N., Scott, R. L., Shi, Y., Sulman, B. N., & Wood, J. D. (2022).
1051 Confronting the water potential information gap. *Nature Geoscience*, *15*(3), 158–164.
1052 https://doi.org/10.1038/s41561-022-00909-2
1053 O'Neill, P. E., Bindlish, R., Chan, S., Chaubell, J., Njoku, E. G., & Jackson, T. J. (2019). *SMAP*
1054 *Algorithm Theoretical Basis Document: Level 2 & 3 Soil Moisture (Passive) Data*
1055 *Products*. Jet Propulsion Laboratory.
1056 Pallardy, S. G., Gu, L., Wood, J. D., Hosman, K. P., & Sun, Y. (2018). *Predawn Leaf Water*
1057 *Potential of Oak-Hickory Forest at Missouri Ozark (MOFLUX) Site: 2004-2020* [Data
1058 set]. ORNLTESSFA (Oak Ridge National Lab's Terrestrial Ecosystem Science Scientific
1059 Focus Area (ORNL TES SFA)). https://doi.org/10.3334/CDIAC/ORNLSFA.004
1060 Rao, K., Anderegg, W. R. L., Sala, A., Martínez-Vilalta, J., & Konings, A. G. (2019). Satellite-
1061 based vegetation optical depth as an indicator of drought-driven tree mortality. *Remote*
1062 *Sensing of Environment*, *227*, 125–136. https://doi.org/10.1016/j.rse.2019.03.026
1063 Rao, K., Williams, A. P., Diffenbaugh, N. S., Yebra, M., & Konings, A. G. (2022). Plant-water
1064 sensitivity regulates wildfire vulnerability. *Nature Ecology & Evolution*, *6*(3), 332–339.
1065 https://doi.org/10.1038/s41559-021-01654-2
1066 Reichle, R. H., De Lannoy, G. J. M., Liu, Q., Ardizzone, J. V., Colliander, A., Conaty, A., Crow,
1067 W., Jackson, T. J., Jones, L. A., Kimball, J. S., Koster, R. D., Mahanama, S. P., Smith, E.
1068 B., Berg, A., Bircher, S., Bosch, D., Caldwell, T. G., Cosh, M., González-Zamora, Á., …
1069 Zeng, Y. (2017). Assessment of the SMAP Level-4 Surface and Root-Zone Soil Moisture
1070 Product Using In Situ Measurements. *Journal of Hydrometeorology*, *18*(10), 2621–2645.
1071 https://doi.org/10.1175/JHM-D-17-0063.1

1072 Renner, M., Brenner, C., Mallick, K., Wizemann, H.-D., Conte, L., Trebs, I., Wei, J.,
1073 Wulfmeyer, V., Schulz, K., & Kleidon, A. (2019). Using phase lags to evaluate model
1074 biases in simulating the diurnal cycle of evapotranspiration: A case study in Luxembourg.
1075 *Hydrology and Earth System Sciences*, *23*(1), 515–535. https://doi.org/10.5194/hess-23-
1076 515-2019
1077 Reyer, C. P. O., Leuzinger, S., Rammig, A., Wolf, A., Bartholomeus, R. P., Bonfante, A., de
1078 Lorenzi, F., Dury, M., Gloning, P., Abou Jaoudé, R., Klein, T., Kuster, T. M., Martins,
1079 M., Niedrist, G., Riccardi, M., Wohlfahrt, G., de Angelis, P., de Dato, G., François, L., …
1080 Pereira, M. (2013). A plant's perspective of extremes: Terrestrial plant responses to
1081 changing climatic variability. *Global Change Biology*, *19*(1), 75–89.
1082 https://doi.org/10.1111/gcb.12023
1083 Shan, X., Steele-Dunne, S., Huber, M., Hahn, S., Wagner, W., Bonan, B., Albergel, C., Calvet,
1084 J.-C., Ku, O., & Georgievska, S. (2022). Towards constraining soil and vegetation
1085 dynamics in land surface models: Modeling ASCAT backscatter incidence-angle
1086 dependence with a Deep Neural Network. *Remote Sensing of Environment*, *279*, 113116.
1087 https://doi.org/10.1016/j.rse.2022.113116
1088 Silva, M., Matheny, A. M., Pauwels, V. R. N., Triadis, D., Missik, J. E., Bohrer, G., & Daly, E.
1089 (2022). Tree hydrodynamic modelling of the soil–plant–atmosphere continuum using
1090 FETCH3. *Geoscientific Model Development*, *15*(6), 2619–2634.
1091 https://doi.org/10.5194/gmd-15-2619-2022
1092 Skelton, R. P., West, A. G., & Dawson, T. E. (2015). Predicting plant vulnerability to drought in
1093 biodiverse regions using functional traits. *Proceedings of the National Academy of*
1094 *Sciences*, *112*(18), 5744–5749. https://doi.org/10.1073/pnas.1503376112

1095 Steele-Dunne, S. C., Friesen, J., & van de Giesen, N. (2012). Using Diurnal Variation in
1096 Backscatter to Detect Vegetation Water Stress. *IEEE Transactions on Geoscience and*
1097 *Remote Sensing*, *50*(7), 2618–2629. https://doi.org/10.1109/TGRS.2012.2194156
1098 Still, C. J., Page, G., Rastogi, B., Griffith, D. M., Aubrecht, D. M., Kim, Y., Burns, S. P.,
1099 Hanson, C. V., Kwon, H., Hawkins, L., Meinzer, F. C., Sevanto, S., Roberts, D.,
1100 Goulden, M., Pau, S., Detto, M., Helliker, B., & Richardson, A. D. (2022). No evidence
1101 of canopy-scale leaf thermoregulation to cool leaves below air temperature across a range
1102 of forest ecosystems. *Proceedings of the National Academy of Sciences*, *119*(38),
1103 e2205682119. https://doi.org/10.1073/pnas.2205682119
1104 Sun, D., & Pinker, R. (2003). Estimation of land surface temperature from a Geostationary
1105 Operational Environmental Satellite (GOES-8). *Journal of Geophysical Research*,
1106 *108*(D11), 4326. https://doi.org/10.1029/2002JD002422
1107 Tang, J., & Zhuang, Q. (2008). Equifinality in parameterization of process-based
1108 biogeochemistry models: A significant uncertainty source to the estimation of regional
1109 carbon dynamics: EQUIFINALITY IN REGIONAL CARBON DYNAMICS. *Journal of*
1110 *Geophysical Research: Biogeosciences*, *113*(G4). https://doi.org/10.1029/2008JG000757
1111 Tindall, J. A., Kunkel, J. R., & Anderson, D. E. (1999). *Unsaturated zone hydrology for*
1112 *scientists and engineers*. Prentice Hall.
1113 Turner, N. C. (1988). Measurement of plant water status by the pressure chamber technique.
1114 *Irrigation Science*, *9*(4), 289–308. https://doi.org/10.1007/BF00296704
1115 Ulaby, F. T., & Long, D. G. (2014). *Microwave radar and radiometric remote sensing*. The
1116 University of Michigan Press.

Vereecken, H., Amelung, W., Bauke, S. L., Bogena, H., Brüggemann, N., Montzka, C., Vanderborght, J., Bechtold, M., Blöschl, G., Carminati, A., Javaux, M., Konings, A. G., Kusche, J., Neuweiler, I., Or, D., Steele-Dunne, S., Verhoef, A., Young, M., & Zhang, Y. (2022). Soil hydrology in the Earth system. *Nature Reviews Earth & Environment*, *3*(9), 573–587. https://doi.org/10.1038/s43017-022-00324-6

Wang, H., Wigneron, J.-P., Ciais, P., Yao, Y., Fan, L., Liu, X., Li, X., Green, J. K., Tian, F., Tao, S., Li, W., Frappart, F., Albergel, C., Wang, M., & Li, S. (2023). Seasonal variations in vegetation water content retrieved from microwave remote sensing over Amazon intact forests. *Remote Sensing of Environment*, *285*, 113409. https://doi.org/10.1016/j.rse.2022.113409

Wang, Y., Braghiere, R. K., Longo, M., Norton, A. J., Köhler, P., Doughty, R., Yin, Y., Bloom, A. A., & Frankenberg, C. (2023). Modeling Global Vegetation Gross Primary Productivity, Transpiration and Hyperspectral Canopy Radiative Transfer Simultaneously Using a Next Generation Land Surface Model—CliMA Land. *Journal of Advances in Modeling Earth Systems*, *15*(3). https://doi.org/10.1029/2021MS002964

Wang, Y., Köhler, P., He, L., Doughty, R., Braghiere, R. K., Wood, J. D., & Frankenberg, C. (2021). Testing stomatal models at the stand level in deciduous angiosperm and evergreen gymnosperm forests using CliMA Land (v0.1). *Geoscientific Model Development*, *14*(11), 6741–6763. https://doi.org/10.5194/gmd-14-6741-2021

Wigneron, J.-P., Jackson, T. J., O'Neill, P., De Lannoy, G., de Rosnay, P., Walker, J. P., Ferrazzoli, P., Mironov, V., Bircher, S., Grant, J. P., Kurum, M., Schwank, M., Munoz-Sabater, J., Das, N., Royer, A., Al-Yaari, A., Al Bitar, A., Fernandez-Moran, R., Lawrence, H., … Kerr, Y. (2017). Modelling the passive microwave signature from land

surfaces: A review of recent results and application to the L-band SMOS & SMAP soil moisture retrieval algorithms. *Remote Sensing of Environment*, *192*, 238–262. https://doi.org/10.1016/j.rse.2017.01.024

Wood, J. D., Gu, L., Hanson, P. J., Frankenberg, C., & Sack, L. (2023). The ecosystem wilting point defines drought response and recovery of a *QUERCUS-CARYA* forest. *Global Change Biology*, *29*(7), 2015–2029. https://doi.org/10.1111/gcb.16582

Wood, J., & Gu, L. (2022). *AmeriFlux FLUXNET-1F US-MOz Missouri Ozark Site* [Data set]. AmeriFlux; Oak Ridge National Laboratory; University of Missouri. https://doi.org/10.17190/AMF/1854370

Wood, J., Gu, L., Hanson, P., Frankenberg, C., & Sack, L. (2022). *Supporting biophysical data for "The ecosystem wilting point defines drought response and recovery of a Quercus-Carya forest"* [Data set]. Zenodo. https://doi.org/10.5281/ZENODO.7477878

Wu, G., Guan, K., Li, Y., Novick, K. A., Feng, X., McDowell, N. G., Konings, A. G., Thompson, S. E., Kimball, J. S., De Kauwe, M. G., Ainsworth, E. A., & Jiang, C. (2021). Interannual variability of ecosystem iso/anisohydry is regulated by environmental dryness. *New Phytologist*, *229*(5), 2562–2575. https://doi.org/10.1111/nph.17040

Xiao, J., Fisher, J. B., Hashimoto, H., Ichii, K., & Parazoo, N. C. (2021). Emerging satellite observations for diurnal cycling of ecosystem processes. *Nature Plants*, *7*(7), 877–887. https://doi.org/10.1038/s41477-021-00952-8

Xu, S., McVicar, T. R., Li, L., Yu, Z., Jiang, P., Zhang, Y., Ban, Z., Xing, W., Dong, N., Zhang, H., & Zhang, M. (2022). Globally assessing the hysteresis between sub-diurnal actual evaporation and vapor pressure deficit at the ecosystem scale: Patterns and mechanisms.

Agricultural and Forest Meteorology, *323*, 109085. https://doi.org/10.1016/j.agrformet.2022.109085

Xu, T., Bateni, S. M., Neale, C. M. U., Auligne, T., & Liu, S. (2018). Estimation of Turbulent Heat Fluxes by Assimilation of Land Surface Temperature Observations From GOES Satellites Into an Ensemble Kalman Smoother Framework. *Journal of Geophysical Research: Atmospheres*, *123*(5), 2409–2423. https://doi.org/10.1002/2017JD027732

Xu, X., Konings, A. G., Longo, M., Feldman, A., Xu, L., Saatchi, S., Wu, D., Wu, J., & Moorcroft, P. (2021). Leaf surface water, not plant water stress, drives diurnal variation in tropical forest canopy water content. *New Phytologist*, nph.17254. https://doi.org/10.1111/nph.17254

Yebra, M., Dennison, P. E., Chuvieco, E., Riaño, D., Zylstra, P., Hunt, E. R., Danson, F. M., Qi, Y., & Jurdao, S. (2013). A global review of remote sensing of live fuel moisture content for fire danger assessment: Moving towards operational products. *Remote Sensing of Environment*, *136*, 455–468. https://doi.org/10.1016/j.rse.2013.05.029

Young, F. J., Caryl A. Radatz, & Curtis A. Marshall. (2001). *Soil survey of Boone County, Missouri*. USDA NRCS.

Yu, Y., Tarpley, D., Privette, J. L., Flynn, L. E., Xu, H., Chen, M., Vinnikov, K. Y., Sun, D., & Tian, Y. (2012). Validation of GOES-R Satellite Land Surface Temperature Algorithm Using SURFRAD Ground Measurements and Statistical Estimates of Error Properties. *IEEE Transactions on Geoscience and Remote Sensing*, *50*(3), 704–713. https://doi.org/10.1109/TGRS.2011.2162338

1183 Yu, Z., Wang, J., Liu, S., Rentch, J. S., Sun, P., & Lu, C. (2017). Global gross primary
1184 productivity and water use efficiency changes under drought stress. *Environmental*
1185 *Research Letters*, *12*(1), 014016. https://doi.org/10.1088/1748-9326/aa5258
1186 Zeng, X., Atlas, R., Birk, R. J., Carr, F. H., Carrier, M. J., Cucurull, L., Hooke, W. H., Kalnay,
1187 E., Murtugudde, R., Posselt, D. J., Russell, J. L., Tyndall, D. P., Weller, R. A., & Zhang,
1188 F. (2020). Use of Observing System Simulation Experiments in the United States.
1189 *Bulletin of the American Meteorological Society*, *101*(8), E1427–E1438.
1190 https://doi.org/10.1175/BAMS-D-19-0155.1
1191 Zhang, Q., Manzoni, S., Katul, G., Porporato, A., & Yang, D. (2014). The hysteretic
1192 evapotranspiration-Vapor pressure deficit relation: ET-VPD hysteresis. *Journal of*
1193 *Geophysical Research: Biogeosciences*, *119*(2), Article 2.
1194 https://doi.org/10.1002/2013JG002484
1195